ORAL PRESENTATION

Sciences/Agriculture/Environment and Technology

Graduate School

Valaya Alongkorn Rajabhat University under the Royal Patronage

INVESTIGATION OF PARAMETERS EFFECT ON RESISTIVE LEAKAGE CURRENT EXTRACTION FOR GAPLESS ARRESTER (MOSA)

Chorphaka Plaengpraphan[1] Nutthaphong Tunthanuch[2]

[1] Programmes of Innovative Engineering
Faculty of Engineering Thammasat university email May_Bp_7047@hotmail.com
[2] Department of Electrical and Computer Engineering
Faculty of Engineering Thammasat university email tanthanuch1@engr.tu.ac.th

ABSTRACT

Currently, there are many methods are used to monitor surge arrester's conditions such as visual inspection, thermal image, partial discharge measurement and leakage current measurement. In order to examine the condition of a surge arrester with high accuracy and more convenience, leakage current measurement is proposed. This method inspects the condition of a surge arrester in online condition that means it does not need to be disconnected the equipment from the power system. The condition of apparatus are investigated by using resistive leakage current component. Up to now, several methods are used to extract the resistive leakage current component and it can be divided into two groups, namely the analysis methods and the graphical methods. Nevertheless, these methods have totally different algorithms, sampling points, waveform characteristics and equivalent models including the effect of voltage harmonics and inconstant frequency may result in the accuracy of resistive leakage current extraction. To verify the accuracy of extracted results, this paper studies the parameters which are voltage harmonics, phase shift, sampling rate and frequency that can affect on resistive leakage current extraction methods for a gapless surge arrester by using three analysis methods comprise of Improve Compensation Method, Harmonic Analysis Method and Current Orthogonality Method. These methods are based on two equivalent models which are simplified and nonlinear models.

With regarding the extracted results on simplified model, the results are clearly showed that inconstant power system frequency directly affects to three different resistive leakage current extraction methods. The magnitude and waveform of resulted currents have errors when the value of power system frequency is not 50 Hz. On the other hand, for nonlinear model, all the parameters that mentioned above affect to extraction methods especially the magnitude and waveform results from Harmonic Analysis Method which had the highest error, compared to lower error from other methods. However, Harmonic Analysis Method is the most suitable method using for current extraction on simplified model because this method has less calculation process and is not complicated. This method is appropriate with the system or device which are limited calculation's speed and lower efficiency such as simple microcontroller. In contrast, Current Orthogonality Method is proper for current extraction on nonlinear model since this method provides the highest accuracy both magnitude and waveform when considered the effect of all parameters.

Keywords: Improve Compensation Method, Harmonic Analysis Method, Current Orthogonality Method, simplified model, nonlinear model

Introduction

Surge arrester is an important protective device which is used to protect other electrical equipment from transient overvoltage for stability and reliability of power system. However, when used, this equipment is subjected to humidity, heat, contamination. These factors may lead to deterioration. [1] Therefore, the monitoring of degradation of this apparatus is necessary. There are various investigation methods to evaluate condition of the arrester such as surge test, thermal image, partial discharge test, insulation resistance test, dissipation factor test and so on. [2] Typically, the most common method is based on the measurement of the leakage current with the separating of the resistive leakage current component. As it is well known that the resistive component of the total leakage current is a good parameter for indicating of the condition of surge arrester. [3] Several methods used to extract the resistive leakage current component and can be classified into two groups, namely the analytical methods and the graphical methods. Nevertheless, these methods have totally different in algorithms, sampling points, waveform characteristics and equivalent models. In addition, effect of voltage harmonics and unstable frequency may affect to the accuracy of resistive leakage current extraction. [4],[5]

To verify the accuracy of the analytical techniques, this paper studies and investigates the parameters which affect on resistive leakage current extraction method for metal oxide surge arrester (MOSA) to offer guidance for choosing the extraction method which is suitable for the measured data or the limitation of each algorithm.

Leakage Current and Extraction Methods

Leakage Current

Leakage current is a small current flowing through surface and into the insulator. In general, the total leakage current $i_t(t)$ flowing through the insulator can be decomposed into two components which are resistive leakage current $i_r(t)$ and capacitive leakage current $i_c(t)$ as given by,

$$i_t(t) = i_c(t) + i_r(t) \tag{1}$$

Extraction Methods

In this paper, total leakage current was extracted by three analytical methods comprise of improve compensation method, harmonic analysis method and current orthogonality method. [6],[7]

Improve Compensation Method (ICM)

$$v_t(t) = V_0 + \sum_{k=1}^{\infty} V_k \sin(k\omega t + \alpha_k) \tag{2}$$

$$i_t(t) = I_0 + \sum_{k=1}^{\infty} I_k \sin(k\omega t + \beta_k) \tag{3}$$

where V_0 is DC component of voltage

I_0 is DC component of leakage current

V_k is k harmonic peak value of voltage

I_k is k harmonic peak value of leakage current
α_k is phase angle of voltage
β_k is phase angle of leakage current
ω is angular frequency

The resistive leakage current can be obtained by,

$$i_{r,n}(t) = i_{t,n}(t) - G_n V_{sf,n}(t) \quad (4)$$

The constant G_n on the right hand side of equation (4) is the compensating coefficient of n harmonic which can be calculated by,

$$\int_0^T \left[v_{sf,n}(t) \times \left(i_{t,n}(t) - G_n v_{sf,n}(t) \right) \right] dt = 0 \quad (5)$$

where $v_{sf,n}(t)$ is *n* harmonic of voltage that 90◦ phase shift with respect to $v_n(t)$
$i_{r,n}(t)$ is *n* harmonic of resistive leakage current
$i_{t,n}(t)$ is *n* harmonic of total leakage current

Harmonic Analysis Method (HAM)

Referred to voltage and leakage current that applied to MOSA, equations can be presented by (1) and (2)
The method suggests that i_r is in-phase with voltage and i_c leads voltage by 90 degree which are represented, respectively, as

$$i_c(t) = \sum_{k=1}^{\infty} I_{c_k} \cos(k\omega t + \alpha_k) \quad (6)$$

$$i_r(t) = I_0 + \sum_{k=1}^{\infty} I_{r_k} \sin(k\omega t + \alpha_k) \quad (7)$$

Based on (1), the total leakage current can be given as,

$$i_t(t) = I_0 + \sum_{k=1}^{\infty} I_{r_k} \sin(k\omega t + \alpha_k) + \sum_{k=1}^{\infty} I_{c_k} \cos(k\omega t + \alpha_k) \quad (8)$$

where I_{r_k} is k harmonic peak value of resistive leakage current
I_{c_k} is k harmonic peak value of capacitive leakage current

From (8), multiplying both sides by $\sin(k\omega t + \alpha_k)$ and integrating over a period, the resistive leakage current can be obtained by,

$$I_{r_k} = I_k[\cos(\beta_k)\cos(\alpha_k) + \sin(\beta_k)\sin(\alpha_k)] \quad (9)$$

Current Orthogonality Method (COM)

This method is based on the orthogonality between resistive leakage current (i_r) and capacitive leakage current (i_c). Assume i'_c is equal to the capacitive leakage current when a capacitor is equal to 1 Farad, then it can be expressed as follows:

$$i'_c(t) = \frac{dv_t(t)}{dt} = \frac{i_c(t)}{C} \quad (10)$$

Integration of the product of leakage currents $i(t)$ and $i'_c(t)$ in a voltage signal period is

$$B = \int_0^T i'_c(t)\, i_t(t)dt \tag{11}$$

By combination, equation (11) can be written as,

$$B = \int_0^T i'_c(t)\left(i_r(t) + Ci'_c(t)\right)dt = C\int_0^T i'_c(t)^2 dt \tag{12}$$

Combining (11) and (12), the actual capacitance (C) is expressed as

$$C = \frac{\int_0^T i'_c(t)\, i_t(t)dt}{\int_0^T i'_c(t)^2 dt} \tag{13}$$

where $i'_c(t)$ is equal to the differential of the voltage signal v(t).
The resistive leakage current is gotten as the following

$$i_r(t) = i_t(t) - Ci'_c(t) \tag{14}$$

Experimental Methods

Surge Arrester Models

In this work, The MOSA could be represented as two equivalent models, simplified and nonlinear models. On the one hand, the simplified model shown in Fig. 1 comprises of a capacitance branch in parallel with a linear resistance branch

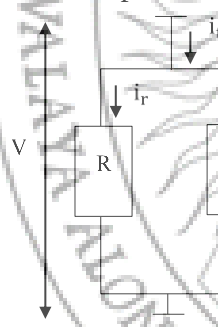

Fig. 1 simplified model

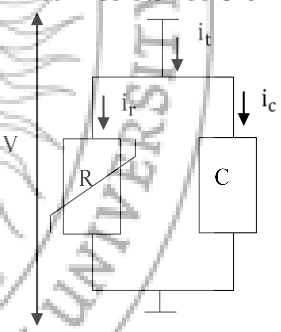

Fig. 2 nonlinear model

The resistance of the leakage current of surge arrester is obtained by volt-ampere method. It is equal to 100 MΩ. Capacitance is 100 pF, test values in high voltage laboratory.

On the other hand, the nonlinear model consists of a capacitance in parallel with a non-linear resistance as shown in Fig. 2.
The relationship between the resistive leakage current and the voltage of MOSA [7] is

$$i_r = \left[\frac{v(t)}{B}\right]^{\alpha} \tag{15}$$

where B,α are constants, with a value of 14.44 and 7, respectively
C is capacitor component, with a value of 100 pF

Influence of the parameters

In this experimental, we applied three harmonics voltage to the arrester models consist of fundamental harmonic voltage, third harmonic voltage and fifth harmonic voltage and we study the four different parameters which are harmonics,

phase angle and frequency of voltage and sampling rate of tested data. Surge arresters that we have studied are used in the 11 kV distribution network. Furthermore, the magnitude and waveform of extracted leakage current results were considered and compared with tested current.

Research Results and Discussion

Voltage Harmonics

The fundamental harmonic voltage and the fifth harmonic voltage were fixed at 1 p.u. (based on system voltage) and 0.02 p.u. while the third harmonic voltage were applied in the range 0.03 p.u. to 0.2 p.u., the fundamental frequency of the voltage signal is 50 Hz, the sampling frequency is 20 kHz and the phase angle of all harmonics voltage are same (equal to 0).

With regarding to simplified model, although the range of the third harmonic voltage was varied, the relative errors of resistive leakage current remained fairly stable and these were lower than 1%. The magnitude and waveform which obtained by three methods were quite the same. In the same way, the relative errors of resistive leakage current of nonlinear model also were lower than 1%. However, the waveform which obtained by HAM had highest distorted. This is the resulted from resistive leakage current calculated by eq. (9) which does not include the effect of nonlinear relationship between voltage and leakage current.

The resistive leakage current's relative errors according to third harmonic voltage are showed in Table 1 and the example of resulted currents are shown in Fig. 3

Table 1: Relative errors according to third harmonic voltage

Models	3rd harmonic voltage	% errors		
		ICM	HAM	COM
Simplified model	0.03	0.00046735	0.00046655	0.00046892
	0.05	0.00042295	0.00042397	0.00042138
	0.1	0.00236693	0.00236809	0.00236537
	0.15	0.00141208	0.00140923	0.00141364
	0.2	0.00377285	0.00377732	0.00377130
Nonlinear model	0.03	0.00002786	0.00002788	0.00001595
	0.05	0.00000648	0.00000649	0.00000334
	0.1	0.00002876	0.00002877	0.00000741
	0.15	0.00009919	0.00009920	0.00000476
	0.2	0.00035276	0.00035276	0.00003260

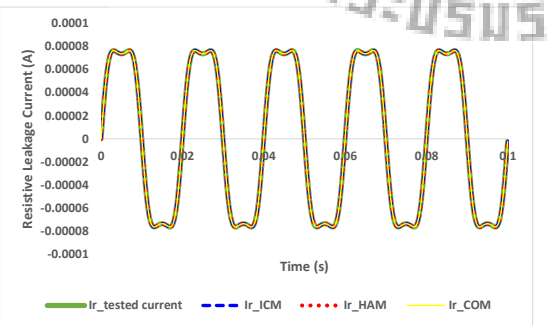

(a) simplified model : 0.2 p.u. V_{3rd}

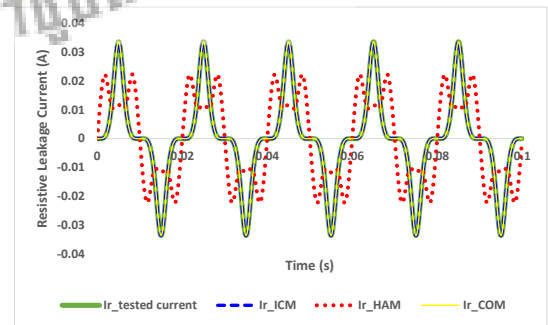

(b) nonlinear model : 0.03 p.u. V_{3rd}

Fig. 3 The resistive leakage current waveform in different third harmonic voltage

Due to the relationship between voltage and nonlinear leakage current, it leads to calculated capacitive leakage current from ICM having the highest errors. These are affected from the compensating coefficient (G_n) which is not a multiply of this constant obtained from fundamental frequency (G_1). However, these errors were lower than 1% and they not affect the current waveform. Relative errors of capacitive leakage current are shown in Fig. 4

Fig.4 capacitive leakage current's relative errors of nonlinear model

Phase Angle of voltage

Referred to voltage harmonics, the fundamental harmonic voltage, the third harmonic voltage and the fifth harmonic voltage were fixed at 1 p.u., 0.2 p.u. and 0.02 p.u., respectively. The fundamental frequency of the voltage signal is 50 Hz, the sampling frequency is 20 kHz. The phase angle of each harmonic that were considered in this topic are shown in Table 2

Table 2: The phase angle of tested voltage

1st Harmonic	3rd Harmonic	5th Harmonic
0˚	30˚	30˚
0˚	60˚	30˚
0˚	180˚	30˚
30˚	30˚	30˚
30˚	60˚	30˚
30˚	180˚	30˚

Despite of varied voltage phase angle, the relative errors of resistive leakage current on simplified model were still lower than 1%. Additionally, the magnitude and waveform of resistive current from three methods were exactly the same.

Turning to nonlinear model, the relative errors of resistive leakage current were not constant. Since the effect of nonlinear relationship between voltage and leakage current, it generates some current phase angle, without respecting phase voltage. These result in resistive leakage current calculated by ICM and HAM having higher error than COM's one. The generated current phase angle not only affect the

magnitude of resistive leakage current but also the resistive leakage current waveform. The relative errors of resistive leakage current according to phase angle are shown in Table 3 while the example of resistive leakage current waveform are shown in Fig.5

Table 3: Relative errors according to voltage phase angle

Models	Phase angle of voltage (1st,3rd,5th)	% errors		
		ICM	HAM	COM
Simplified model	0˚,30˚,30˚	0.00259962	0.00260421	0.00257955
	0˚,60˚,30˚	0.00066689	0.00066783	0.00061440
	0˚,180˚,30˚	0.00037512	0.00037007	0.00037049
	30˚,30˚,30˚	0.00022847	0.00022186	0.00092777
	30˚,60˚,30˚	0.00070239	0.00070558	0.00005248
	30˚,180˚,30˚	0.00237269	0.00237876	0.00234954
Nonlinear model	0˚,30˚,30˚	11.03580284	11.03580333	0.00001862
	0˚,60˚,30˚	15.68709590	15.68709653	0.00000941
	0˚,180˚,30˚	3.42265003	3.42265026	0.00003327
	30˚,30˚,30˚	17.07250972	17.07251130	0.00000410
	30˚,60˚,30˚	16.38705457	16.38705638	0.00000736
	30˚,180˚,30˚	9.39255366	9.39255519	0.00000932

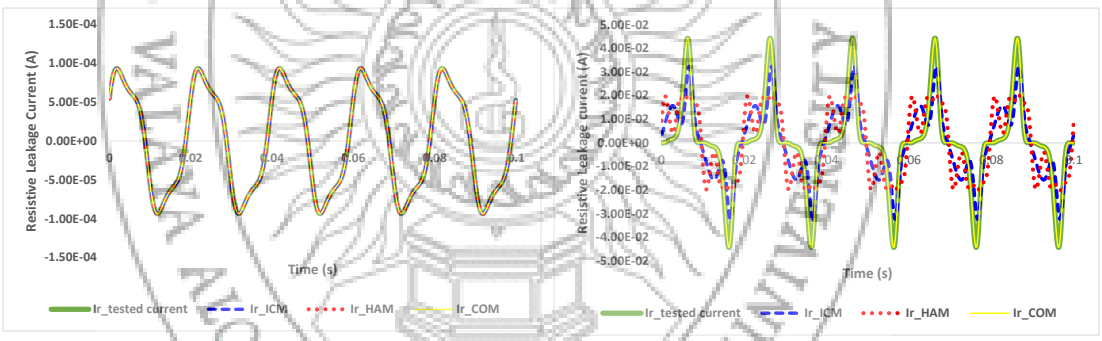

(a) simplified model : 30˚,30˚,30˚ (b) nonlinear model : 0˚,60˚,30˚

Fig. 5 The resistive leakage current waveform in different phase angle

Sampling Frequency

The fundamental harmonic voltage, the third harmonic voltage and the fifth harmonic voltage were fixed at 1 p.u., 0.2 p.u. and 0.02 p.u., respectively. The fundamental frequency of the voltage signal is 50 Hz. The phase angle of all harmonics voltage are same (equal to 0˚) and the sampling frequencies are varied from 2,500 to 160,000 kHz.

The resistive leakage current's relative errors of both models had the same trend. Errors were lower than 1% and the computed results are shown in Table 4. Nevertheless, resistive leakage current waveform of nonlinear model from HAM had a distortion. As described above in 4.1, it does not include the effect of harmonic in system voltage. The example of resulted currents are shown from Fig. 6

Table 4: Relative errors according to sampling frequency

Models	Sampling frequency (Hz)	% errors		
		ICM	HAM	COM
Simplified model	2,500	0.00830057	0.00843032	0.00602976
	5,000	0.00503715	0.00509577	0.00496151
	10,000	0.00588156	0.00589937	0.00588774
	20,000	0.00377285	0.00377732	0.00377130
	40,000	0.00004168	0.00004033	0.00004631
	80,000	0.00079965	0.00079875	0.02081857
	160,000	0.00003396	0.00003334	0.00998631
Nonlinear model	2,500	0.00037892	0.00040198	0.00008170
	5,000	0.00034839	0.00035026	0.00003006
	10,000	0.00034237	0.00034250	0.00002230
	20,000	0.00035276	0.00035276	0.00003260
	40,000	0.00033839	0.00033839	0.00001821
	80,000	0.00032338	0.00032338	0.00009032
	160,000	0.00031016	0.00031016	0.00005679

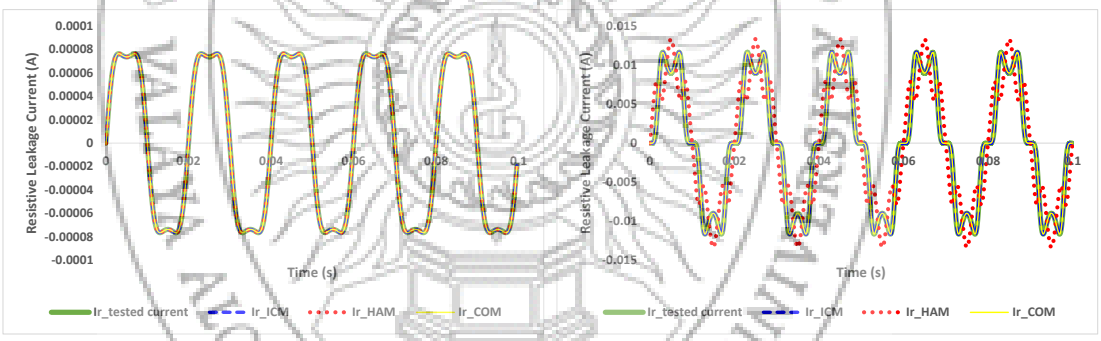

(a) simplified model : 2,500 Hz (b) nonlinear model : 160,000 Hz

Fig. 6 The resistive leakage current waveform in different sampling frequency

Looking at the capacitive leakage current's relative errors, they were reduced when sampling frequency increased, especially ICM and COM. These can be explained by the accuracy of numerical integration, increasing with the number of sampling point. However, these errors not affected the magnitude and the waveform of resistive leakage current. Typically, the magnitude of capacitive leakage current is very small, compared to the resistive leakage current. The relative errors of capacitive leakage current are showed in Fig.7

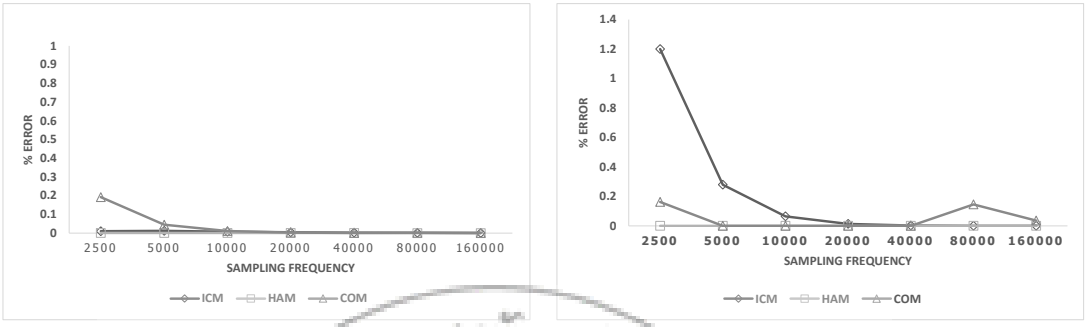

(a) simplified model (b) nonlinear model

Fig. 7 Relative errors of capacitive leakage current in different sampling frequency

Frequency of voltage

The fundamental harmonic voltage, the third harmonic voltage and the fifth harmonic voltage were fixed at 1 p.u., 0.2 p.u. and 0.02 p.u., respectively. The sampling frequency is 20 kHz. The phase angle of all harmonics voltage are same (equal to 0̊) and the fundamental frequency of the voltage signal is varied between 49 and 51 Hz. The relative errors of resistive leakage current are shown in Table 5 and the example of resulted leakage current are shown from Fig. 8

Table 5: Relative errors according to frequency of voltage system

Models	Frequency of voltage system	% errors		
		ICM	HAM	COM
Simplified model	49	2.29676781	2.29676215	21.63050885
	49.5	0.69079064	0.69078542	6.35594543
	50	0.00377285	0.00377732	0.00377130
	50.5	0.56552408	0.56551870	6.83149751
	51	2.22597014	2.22596474	25.36780170
Nonlinear model	49	24.34589450	24.34589528	0.64222576
	49.5	14.74428815	14.74428859	0.33446001
	50	0.00035276	0.00035276	0.00003260
	50.5	14.80568270	14.80568308	0.33172779
	51	24.93370307	24.93370392	0.67405236

From Table 5, it can be obviously seen that the relative errors of resistive leakage current had a higher value when power system frequency is not equal to the line frequency (50 Hz). The reason for higher value is that peak value of voltage and leakage current in Eq. (2) and Eq. (3) are not consistent with the values of tested signals.

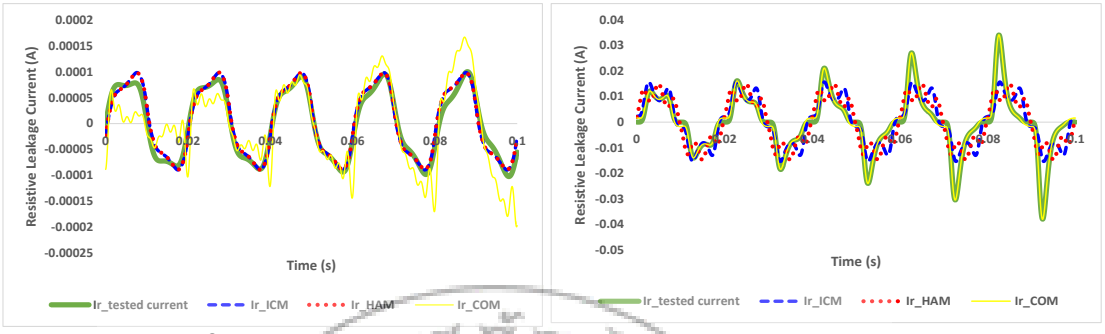

(a) simplified model : 49 Hz (b) nonlinear model : 50.5 Hz

Fig. 8 The resistive leakage current waveform in different frequency of voltage

Conclusion

This paper studies the parameters that can affect the three extraction method. From the extracted results on a simplified model, the results are clearly showed that all parameters that were studied not affect three different extraction methods, with the exception of power frequency. Unstable system frequency directly affect all extraction methods. The magnitude and waveform of resulted currents had errors when the value of power system frequency was not equal to 50 Hz. On the other hand, for a nonlinear model, all the parameters affect the extraction methods especially the magnitude and waveform results from HAM which had the highest errors, compared to other methods. However, HAM is the most suitable method using for current extraction on a simplified model because this method has less complexity and calculation process. It is appropriate for a system or device which is limited by processor speed and little memory. In contrast, COM provides the highest accuracy both magnitude and waveform when it calculate on a nonlinear model.

Acknowledgement

This work is supported by the department of electrical and computer engineering, faculty of engineering, Thammasat university.

References

Muhammad Amin, Salman Amin & Muhammad Ali (2009). Monitoring of Leakage Current for Composite Insulators and Electrical Devices. **Adv.Mater.Sci.** 21, 75-89.

Kuffel, E., Zaengl, W., & Kuffel, J. (2000). **High Voltage Engineering Fundamentals 2nd edition**. Oxford : Newnes.

J. Lundquist, L. Stenström, A. Schei, & B. Hansen (1990). New method for measurement of the resistive leakage currents of metal-oxide surge arresters in service. **IEEE Trans. Power Del**. 5(4), 1811–1822.

Hanxin Zhu & M.R. Raghuveer (1999). Influence of Harmonics in System Voltage on Metal Oxide Surge Arrester Diagnostics. **Conference on Electrical Insulation and Dielectric Phenomenoa**, 542-545.

Hanxin Zhu, M.R. Raghuveer & Senior Member (2016). Influence of Representation Model and Voltage Harmonics on Metal Oxide Surge Arrester Diagnostics. **IEEE Transactions on Power Delivery**. (16).

C. Plaengpraphan & N. Tanthanuch (2015). The Development of Leakage Current Measurement System for High Voltage Equipment. **The 4th International Symposium on Engineering, Energy and Environments**, 135-141.

Zhi-niu Xu, Li-juan Zhao, Ao Ding, & Fang-cheng Lü (2013). A Current Orthogonality Method to Extract Resistive Leakage Current of MOSA. **IEEE Transactions on Power Delivery**. 28(1), 93-101.

COMBINED SEISMIC REFLECTION AND MASW METHOD TO CHARACTERIZE THE SUBSURFACE NEARBY HAT YAI BASIN

Pattawee Srirasa,[1] Sawasdee Yordkayhun,[2] Kamhaeng Wattanasen[3]

[1] Department of Physics, Faculty of Science, Prince of Songkla University pattawee.s@hotmail.com
[2] Department of Physics, Faculty of Science, Prince of Songkla University sawasdee.y@psu.ac.th
[3] Department of Physics, Faculty of Science, Prince of Songkla University kamhaeng.w@psu.ac.th

ABSTRACT

Seismic reflection and multichannel analysis of surface wave (MASW) method were conducted nearby the boundary of Hat Yai basin to characterize the subsurface and determine the depth to bedrock. A 1 km survey line of seismic reflection was acquired and processed to create a seismic section. The presence of surface wave in the same dataset allowed us to study the shear wave velocity distribution in the subsurface. It was found that the distribution of V_s in the shallow subsurface is interpreted to be Quaternary sediment cover of clay, sand, and gravel. A coherent horizon present in the seismic section at approximately 50 m depth is interpreted to be the bedrock in this area. The depth obtained from the seismic section agreed with the well information.

Keywords: Seismic reflection, MASW, Bedrock

Introduction

Hat Yai basin is a sedimentary basin in peninsular southern of Thailand. It is located approximately between longitude $100^{o}15'E$ and$100^{o}30'E$, and latitudes $6^{o}30'N$ and $7^{o}15'N$. The northern border is connected to the Songkhla Lake and bounded by the Gulf of Thailand. The southern border is bounded by the Thai-Malaysian border. Hat Yai city is located at the center of this basin. The structure of Hat Yai basin is thought to be a graben whereas the hill ranges and the small basins east of the graben are parts of a horst (Figure 1).

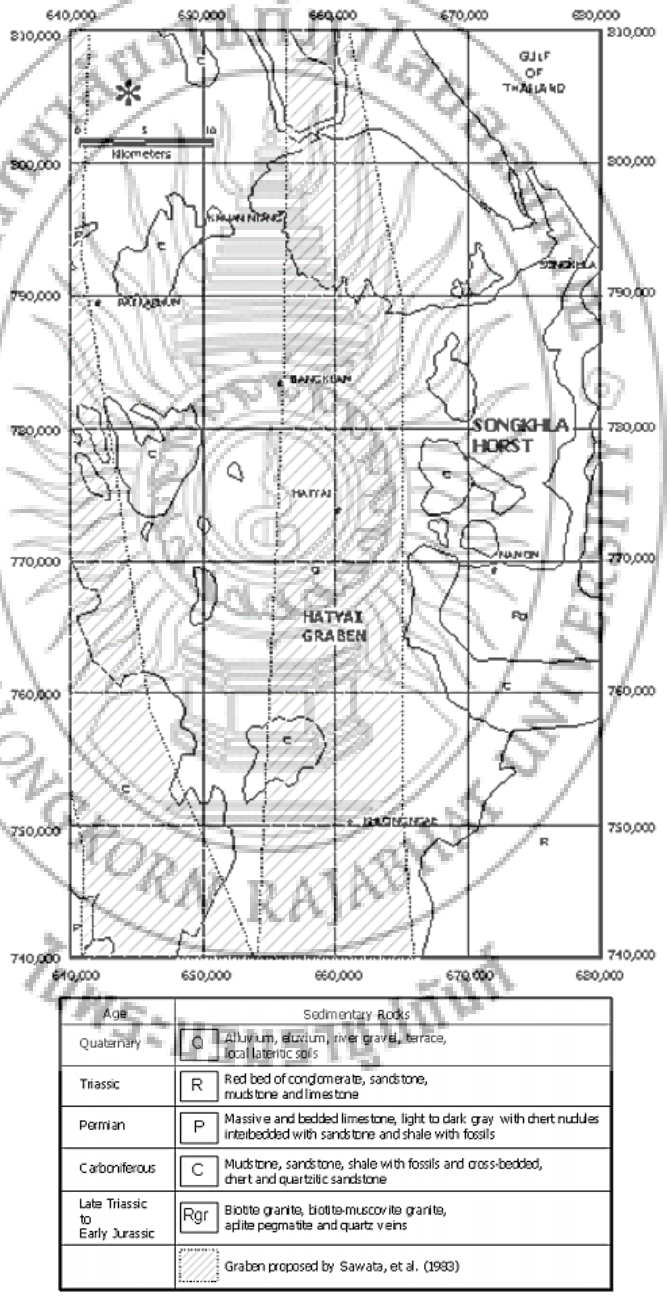

.

Figure 1. Geological map and Graben/host structures within the study area (*Lohawijarn*, 2005).

Geophysical study based on gravity measurement revealed that Hat Yai basin was found to be about 1 km deep at its deepest, 60 km long and 20 km wide (Figure 1). Its' boundary may not extend southward to Malaysia or northward to the Gulf of Thailand (*Lohawijarn*, 2005). However, the spatial resolution of gravity model is limited due to the spacing between gravity measuring points were about 1-2 km. This resulted in less reliable of the boundaries and characteristic of the bedrock in Hat Yai basin. To obtain the detailed information regarding the basin boundaries and the depth to bedrock, the seismic reflection method and multichannel analysis of surface wave (MASW) are combined to fulfill the information about the subsurface.

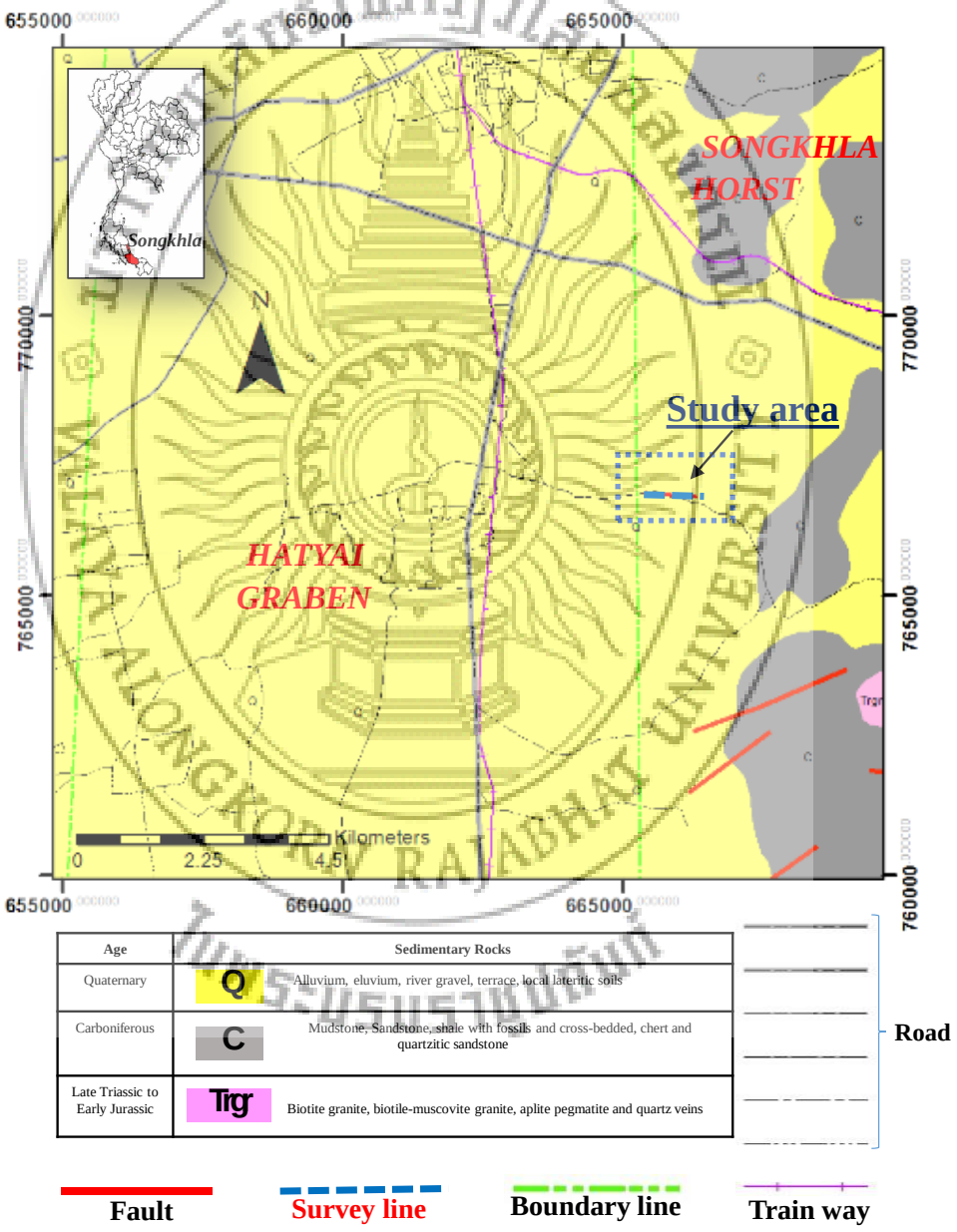

Figure 2. Geological map of the study area showing seismic survey lines.

Seismic methods have been widely used in detecting and mapping subsurface features, especially the layered sedimentary sequences in search of oil and gas

reservoirs. The advantage of seismic methods over other geophysics techniques are due to their high accuracy, high resolution, deeper penetration, and the variety of applications including mapping of the structures, faults, and compaction of various layers. Since the engineering and environmental problems are located at shallow depths, high-resolution seismic reflection method, has been applied to map shallow subsurface structures, depth of water tables, and identification of engineering related problems (*Al-Anezi et al.*, 2013).

The MASW method is the seismic survey method that effectively used to evaluate the stiffness of the ground. This method deals with analysis of surface waves in the lower frequencies and uses for the shallower depth range of investigation (*Park et al*., 2005). For understanding the subsurface structures the two methods are combined to classify layering of subsurface nearby the Hat Yai basin boundary (Figure 2).

Objectives

The objective of this survey is to characterize the subsurface structures and to determine the depth to bedrock nearby the boundary of Hat Yai basin.

Methods

Reflection seismic and MASW are the geophysical methods use for this study. Reflection seismic method depends on the existence of discrete velocity and density change in the subsurface. Discrete changes in seismic velocity or mass density are known as acoustical contrasts. The measure of acoustical contrast is generally known as acoustic impedance, which is the product of mass density and seismic velocity $(Z = \rho V)$. Hence this method involves identifying the boundaries of the layered geologic unit.

The signal intensity of seismic wave is directly related in a variation of the reflection coefficient (R) as expressed in equation 1.

$$R = \frac{\rho_2 V_2 - \rho_1 V_1}{\rho_2 V_2 + \rho_1 V_1} \qquad (1)$$

Where ρ_1 and ρ_2 are density of media 1 and media 2, V_1 and V_2 are the seismic velocity in media 1 and media 2, respectively.

The Multichannel Analysis of Surface Wave (MASW) method deals with analysis of surface waves to generate the shear-wave velocity (V_s) model. Shear modulus obtained from Vs is directly linked to a material's stiffness of the ground for earthquake and geotechnical engineering (*Park et al*., 2005). For the shear wave propagation in elastic media V_s is given by equation 2

$$V_s = \sqrt{\frac{\mu}{\rho}} \qquad (2)$$

Where μ is shear modulus and ρ is medium density.

Data acquisition

A seismic survey line as shown in Figure 2 was acquired in June 2016. The survey line is oriented west to east with the total lengths of 900 m. The survey line is on transportation roads where the traffic was quiet, simplifying the data acquisition.

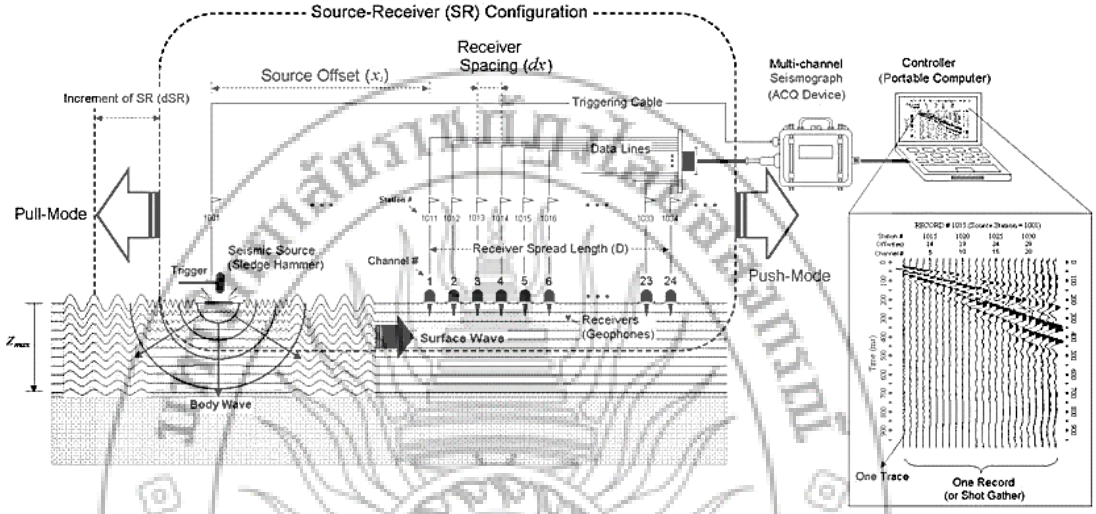

Figure 3. Schematic of the seismic reflection and active MASW field survey (*Park et al.*, 2005).

For seismic reflection data acquisition, common midpoint geometry (CMP) were recorded with 24-channel Geometric SmartSeis seismic recorder using sampling interval and record length of 0.5 ms and 1024 ms, respectively (Figure 3). 24-vertical geophones (natural frequency of 14 Hz) were deployed into the surface with 5 m spacing, connected with roll along system. The source was 10 kg sledgehammer with 5 m spacing, resulting in a 12 common depth point (CDP) fold of coverage. The optimum window for data recording is tested and 30 m offset appeared to be appropriated.

Data processing

Geophysical data processing is aimed to construct high quality images of subsurface and make it suitable for the structural interpretation.

The seismic data were processed using *GLOBE CLARITAS Version 5.5* software developed by the Geological & Nuclear (GNS Science), New Zealand. A basic processing to establish seismic section, following Hunter et al. (1984), Miller (1992) and Yilmaz (2001) is given in Table 1.

In this study, seismic section will be correlated with available geologic information for the interpretation.

Table 1. Data processing step

Processing Step	Description and parameters
1. Setup of field geometry	Assign input shot location and receiver locations into headers
2. Editing bad traces	Remove bad traces
3. Elevation statics and refraction statics	Calculate static correction based on near surface models and elevations
4. Band-pass filtering	Minimum phase Butterworth filtering f_c = 20, 40, 100, 200 Hz, Design Amplitude = 0, 1, 1, 0
5. Automatic gain control (AGC)	Adjust reflection amplitude using 250 ms window
6. Bottom mute	Zero data in the ground roll rang
7. CMP sorting	Sort data by common midpoint number
8. Velocity analysis	Find velocity value that fit layers
9. NMO correction	Apply stacking velocity function including 70% stretch mute
10. Stack	
11. Relative trace balancing	0-512 ms range

For the MASW data processing, SurfSeis software version 4 developed by Kansas Geological Survey (KGS) were used. Each shot record was transformed from the time domain into the frequency domain using Fourier Transform technique in order to estimate a specific dispersion curves (phase velocity versus frequency). An iterative inversion method performed on the dispersion curves resulted in 1-D shear-wave velocity profiles (Figure 4). The processing step of MASW is briefly described in Table 2.

Table 2. Processing steps of MASW.

Processing step	Detail
1.Data import	Convert SEG2 format into KGS format
2.Assign geometry	Assign shot location and receiver location
3.Editing	Kill dead traces
4. High cut filtering	Remove high frequency noises
5.Dispersion analysis	Transformed the time-space (t-x) domain into the frequency-phase velocity (f-v) domain
6.Inversion	Create 1D shear wave velocity profile

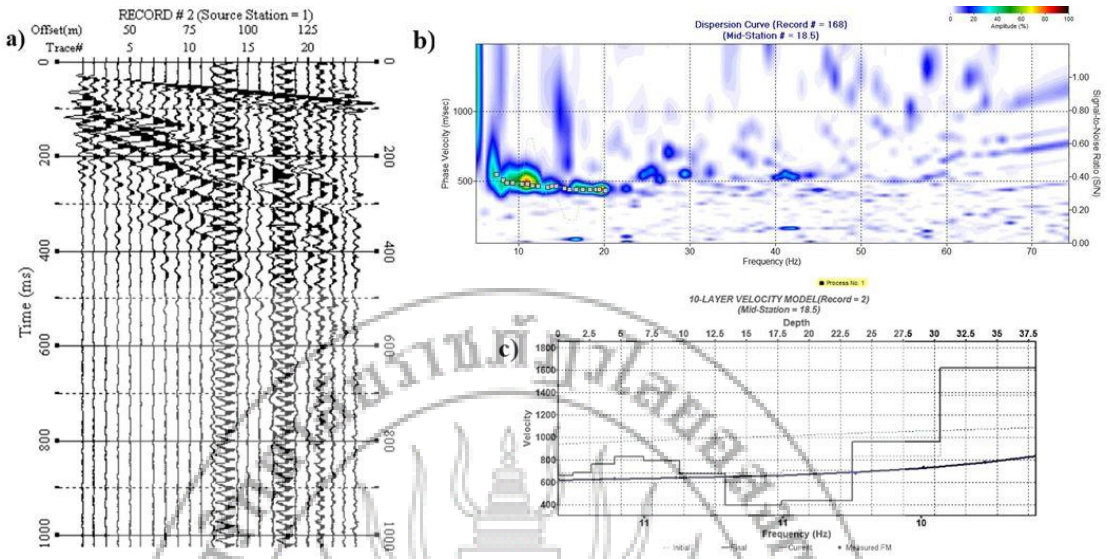

Figure 4. MASW data processing steps a) Raw shot record in time domain b) Dispersion curve, and c) 1D shear wave velocity profile by inversion method.

Results

The interval velocity, amplitude and continuity of the seismic horizons are described and used to classify the sediments and bedrock following the procedure of seismic facies interpretation. Interval velocities of the layer present in the seismic section as shown in Figure 5b were found in a range of 900-3000 m/s. Coherent reflectors are clearly seen at depth of about 50 m and 100 m, respectively. The discontinuities of reflectors are found in the range of about 275-325 m and 625-675 m along the survey line, respectively.

For MASW analysis, the distribution of V_s as shown in Figure 5a can be classified as 2 layers. The first layer is characterized by low velocities of 200-800 m/s with a thickness of about 25 m. The deeper layer is characterized by velocity of higher than 900 m/s at depth below about 30 m.

Discussion and conclusion

Combining stacked depth section and V_s distribution section show sequence of sedimentary units of the subsurface in the depth of 150 m. 2-D shear-wave velocity (V_s) provide information on the internal structures of Quaternary sediments at shallow depth. The first layer is characterized by low velocities of 200-800 m/s with a thickness of 30 m. This layer is interpreted to be Quaternary sediment cover of clay, sand, and gravel. The deep layer about 30-40 m that is characterized by the velocity of higher than 800 m/s may correspond to unconsolidated sedimentary layer because of the variability of the Vs distribution of this layer (Figure 5c). The seismic section along with borehole information from wells logs located approximately 2 km west of the survey line was successfully used to map bedrock. However, the large distance between the boreholes and the survey line means that these logs can be used only as a very general guide in the interpretation of seismic data. The bedrock reflection is clearly present in the seismic section at 50 m depth where the strong impedance contrasts between the sediments and the hard rock (Figure 5d). This probably reveals the Quaternary basement overlying the Carboniferous sedimentary unit and below this

layer at depth 100 m, the quite amplitude reflector is interpreted to represent the bedrock (Indicated by the well screen position of the borehole). However, the shape and characteristics of the reflector vary along the line at this layer. These changes may be attributed to the nature of the transition from sediments to the bedrock.

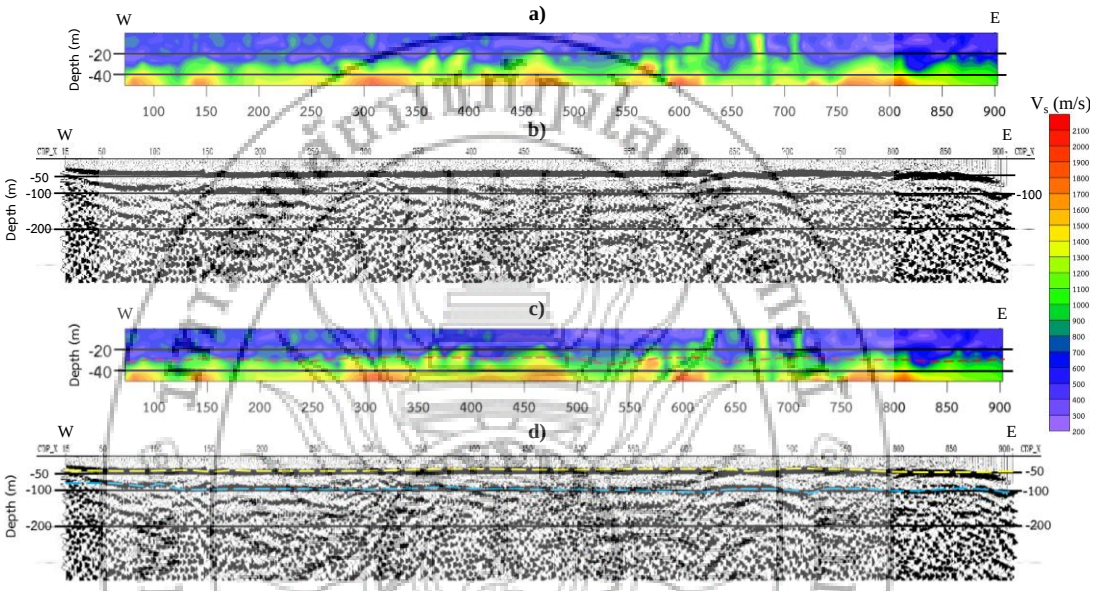

Figure 5. a) The MASW cross section, b) The seismic cross section, c) The MASW cross section after interpretation and d) The seismic cross section after interpretation. The dash line marked the boundary between 2 layers.

Acknowledgement

The author would like to thank the Graduate School at Prince of Songkla University for grant support. Department of Physics and Geophysics Research Center, Faculty of Science are thanked for equipment support. Many thanks graduate students who help, encourage and support during the field work.

References

Al-Anezi, G.T., AlMalki, M., Alkhalifa, T. (2013). Mapping of bedrock using the high-resolution seismic reflection technique at Wadi Al DAwasir Region. *Arabian* **Journal of Geosciences**. 6, 235-245.

Hunter, J. A., Pullan, S. E., Burns, R. A., Gagne, R. M., Good, R. L. (1984). Shallow seismic reflection mapping of the overburden-bedrock interface with the engineering seismograph: some simple techniques. **Journal of Geophysics**. 49, 1381-1385.

Lohawijarn, W. (2005) Potential ground water resources of Hat Yai Basin in Peninsular Thailand by gravity study. **Songklanakarin Journal of Science and Technology**. Sci. Technol., 27(3), 633-647.

Miller, R. (1992). Normal moveout stretch mute on shallow-reflection data. ***Journal of Geophysics*, 57.** 1502–1507.

Park, C. B., Miller, R. D., Ryden, N., Xia, J., and Ivanov, J. (2005). Combined use of active and passive surface wave. *Journal of Engineering and Environmental Geophysics*, 10, 323-334.

Yilmaz, Ö., (2001). *Seismic data analysis: processing, inversion and interpretation of seismic data* . 2nd ed. Tulsa: Society of Exploration Geophysicists.

MATHEMATICAL DEMONSTRATION ON NEUTRON THERMALIZATION BY A RICH H-ATOM POLYMER MATERIALS, PETE FIBER

Sarayut Khemngern

Department of Nuclear Engineering, Faculty of Engineering, Chulalongkorn University
[sarayutk@outlook.co.th]

ABSTRACT

Neutrons would be thermalized by some rich H-atom polymer materials such as polyethyleneterephthalate, PETE fibers because mathematical demonstration has proved neutron thermalization clearly. Vector diagram analysis, law of momentum conservation and law of mechanical energy conservation were also used in this mathematical physics proving. According to the result, writer found that, all energy from neutrons would be transferred out of neutrons into proton particles.

Keywords: Neutron Thermalization, Polymer Materials, Mathematical Demonstration

Introduction

In the future, researcher will use polyethyleneterephthalate, PETE fibers for neutron attenuation in order to make shielding concrete materials that will be applied in the nuclear power plant or in the hospital. Because neutron particles are normally dangerous to human body such as they will affect blood system or tissue system as be cancer (Cember, 1992).This polymer material (PETE) was selected because it has high ratio of H-atom per molecule (Odian, 2004). Researcher expected that this polymer will be used for neutron attenuation effectively. In the similarity procedures of (Lamarsh, 1975) and (Jewett/Serway, 2008), Vector diagram analysis, law of momentum conservation and law of mechanical energy conservation were also applied in this mathematical physics expressions as physiochemical hypothesis.

Analytical Procedures

A simply situation can be considered below; first, a neutron mass m has an initial energy and linear momentum E_1 and $\vec{P}_1$ respectively. And then, it moves to collide with a rest proton mass M which has no an initial energy and linear momentum. After collision, the neutron scattered from the central line with an angle θ_1 which leads to E_2 and $\vec{P}_2$ remaining, whereas the proton mass M remains E_A and $\vec{P}_A$ which has θ_2 as a scattered angle.

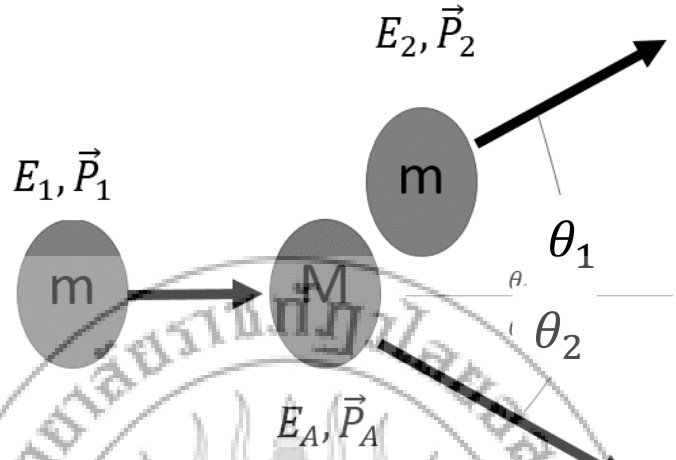

Figure 1: a proton is collided by a neutron

According to the law of energy conservation; $E_1 = E_2 + E_A$ and According to the law of linear momentum conservation; $\vec{P}_1 = \vec{P}_2 + \vec{P}_A$ Then, we can rewrite figure 1 to the figure 2 as a vector illustration.

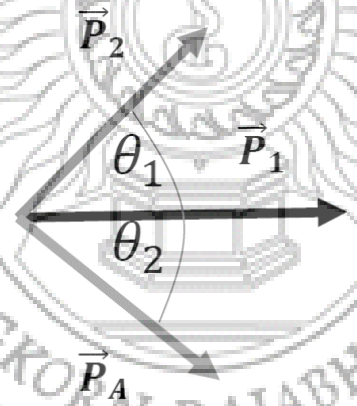

Figure 2: momentum expression as vector diagram

Forasmuch, the cosine's law can be applied to from the new mathematical relation;

$$P_A^2 = P_1^2 + P_2^2 - 2P_1P_2\cos\theta_1 \quad \text{----- (1)}$$

According to the classical mechanics, the quantity of momentum can be written as

$$P = mv$$

Thus

$$P_A = Mv_A$$

$$P_A^2 = (Mv_A)^2$$

$$P_A^2 = M^2v_A^2$$

------- (2)

Since $E_A = \frac{1}{2}Mv_A^2$

So $v_A^2 = \frac{2E_A}{M}$

------- (3)

Substitute (3) into (2)

$$P_A^2 = M^2 \left(\frac{2E_A}{M}\right)$$

$$P_A^2 = 2ME_A$$

------- (4)

In the same way, using the previous procedure; now it can be derived as

$$P_1^2 = 2mE_1$$

------- (5)

And $P_2^2 = 2mE_2$

------- (6)

Substitute (4), (5) and (6) into (1);

$$2ME_A = 2mE_1 + 2mE_2 - 2\sqrt{2mE_1}\sqrt{2mE_2}\cos\theta_1$$

$$2ME_A = 2mE_1 + 2mE_2 - 2(2)m\sqrt{E_1E_2}\cos\theta_1$$

Multiply by $\frac{1}{2}$ both sides

So, $ME_A = mE_1 + mE_2 - 2m\sqrt{E_1E_2}\cos\theta_1$ ------- (7)

It decisively that $\frac{M}{m} \equiv A$

Where M is the target atomic mass

m is the neutron mass (≈1 a.m.u.)

And A is an atomic mass number

So, $M = A$ ------ (8)

Substitute (8) into (7);

$$AE_A = mE_1 + mE_2 - 2m\sqrt{E_1E_2}\cos\theta_1$$

$$AE_A = (1)E_1 + (1)E_2 - 2(1)\sqrt{E_1E_2}\cos\theta_1$$

$$AE_A = E_1 + E_2 - 2\sqrt{E_1E_2}\cos\theta_1 \quad \text{----}$$

-- (9)

Then, substitute $E_A = E_1 - E_2$ into (9)

$$A(E_1 - E_2) = E_1 + E_2 - 2\sqrt{E_1E_2}\cos\theta_1$$

$$AE_1 - AE_2 = E_1 + E_2 - 2\sqrt{E_1E_2}\cos\theta_1$$

$$-AE_2 - E_2 + 2\sqrt{E_1E_2}\cos\theta_1 + AE_1 - E_1 = 0$$

$$AE_2 + E_2 - 2\sqrt{E_1E_2}\cos\theta_1 - AE_1 + E_1 = 0$$

$$(A+1)E_2 - 2\sqrt{E_1E_2}\cos\theta_1 - (A-1)E_1 = 0$$

$$(A+1)E_2 - 2\sqrt{E_1}\sqrt{E_2}\cos\theta_1 - (A-1)E_1 = 0$$

$$(A+1)\sqrt{E_2}^2 - 2\sqrt{E_1}\sqrt{E_2}\cos\theta_1 - (A-1)E_1 = 0 \quad \text{-----}$$

(10)

Then, the following quadratic equation below can be used to find the roots of the former equation (10);

$$x = \frac{-b \pm \sqrt{b^2 - 4ac}}{2a}$$

$$(A+1)\sqrt{E_2}^2 - 2\sqrt{E_1}\sqrt{E_2}\cos\theta_1 - (A-1)E_1 = 0$$

$$\sqrt{E_2} = \frac{2\sqrt{E_1}\cos\theta_1 \pm \sqrt{\left(2\sqrt{E_1}\cos\theta_1\right)^2 - 4(A+1)(-(A-1))E_1}}{2(A+1)}$$

$$\sqrt{E_2} = \frac{2\sqrt{E_1}\cos\theta_1 \pm \sqrt{4E_1\cos^2\theta_1 + 4(A+1)((A-1))E_1}}{2(A+1)}$$

$$\sqrt{E_2} = \frac{2\sqrt{E_1}\cos\theta_1 \pm \sqrt{4E_1\cos^2\theta_1 + 4(1+1)((1-1))E_1}}{2(1+1)}$$

$$\sqrt{E_2} = \frac{2\sqrt{E_1}\cos\theta_1 \pm \sqrt{4E_1\cos^2\theta_1 + 4(2)(0)E_1}}{2(2)}$$

$$\sqrt{E_2} = \frac{2\sqrt{E_1}\cos\theta_1 \pm \sqrt{4E_1\cos^2\theta_1 + 0}}{2(2)}$$

$$\sqrt{E_2} = \frac{2\sqrt{E_1}\cos\theta_1 \pm \sqrt{4E_1\cos^2\theta_1}}{4}$$

$$\sqrt{E_2} = \frac{2\sqrt{E_1}\cos\theta_1 \pm 2\sqrt{E_1}\cos\theta_1}{4}$$

$$\sqrt{E_2} = \frac{\sqrt{E_1}\cos\theta_1 \pm \sqrt{E_1}\cos\theta_1}{2}$$

$$\sqrt{E_2} = \frac{1}{2}\left[\sqrt{E_1}\cos\theta_1 \pm \sqrt{E_1}\cos\theta_1\right]$$

$$E_2 = \frac{1}{4}\left[\sqrt{E_1}\cos\theta_1 \pm \sqrt{E_1}\cos\theta_1\right]^2$$

$$E_2 = \frac{1}{4}\left[\sqrt{E_1}(\cos\theta_1 \pm \cos\theta_1)\right]^2$$

Since the term $\cos\theta_1 + \cos\theta_1$ cannot be written due to physics' principle, thus use

$$E_2 = \frac{1}{4}\left[\sqrt{E_1}(\cos\theta_1 - \cos\theta_1)\right]^2$$

$$E_2 = \frac{1}{4}\left[\sqrt{E_1}(0)\right]^2$$

$$E_2 = 0 \qquad \text{---------} \quad (11)$$

Result and Discussion

According to the previous mathematical demonstration hypothesis, it shows that all energy from neutron will be transferred out of a neutron into proton particle as can be seen from equation (11). Because polyethylene family is one of the rich H-atom polymers, so they probably can thermalize a neutron satisfactory which agree with (Cember, 1992) that used polyethylene for neutron shielding.

References

Cember. (1992). **introduction to health physics.** New York: Pergamon Press.

Jewett/Serway. (2008). **physics for scientists and engineers with modern physics.** Callifornia: Thomson Books / Cole.

Lamarsh, J. R. (1975). **introduction to nuclear engineering.** London: Addison-Wesley Publishing Company.

Odian, G. (2004). **principle of polymerization.** New York: a John Wiley & Sons.

SUITABLE OF THE GARDEN PLANT POSITIONING FOR REDUCING THE WIND SPEED IN HOSPITAL

Nareerat Bourbud[1] and Phitchayakorn Techato [2]

[1] Nareerat Bourbud Faculty Environmental Management Prince of Songkla University
aom_charmer@hotmail.co.th
[2] Phitchayakorn Techato Faculty Sport Science and Health Institute of Physical Education Trang

ABSTRACT

This research is a study of wind blowing through the garden plant at corridor of patient room in hospital in of order to be used as guidelines for the green areas of hospitals. The *Sansevieria spp.* and *Aechmea fasciata.* is suitable to be used because of the drought-resistant plants of both species need water small amounts and can be maintained easily. The experiment for *Sansevieria spp.* and *Aechmea -fasciata.* is set at the height of 30, 40, and 50 cm in one row, two row and two row of zigzag. The results showed that the speed of the wind blowing through the *Sansevieria spp.* is higher compared with the *Aechmea fasciata.* due to the slender or thinner of the leaves. The plants height at 30 cm let the wind blow through better than at the 40 cm and 50 cm plant, respectively. In planting layout, the wind blow through one row of plant better than two rows and two rows of zigzag. It can be concluded that at the height of 30 cm of *Sansevieria spp.* planting in one row is the most suitable to be used as garden plant to be planted in the corridor balcony of the hospital.

Keywords: Sansevieria spp., Aechmea Fasciata., Wind Velocity, Building

Introduction

Due to the current global warming, the average global temperature tends to increase 1.1 to 6.4 degree Celsius. One reason of the temperature rise is the green-house effect which is anthropogenic activities such as coal burning, fuel burning and specific chemical emissions. Nowadays, more air conditioners are used for Thai architecture because of the hot and humid climate in Thailand is not in the comfort zone or thermal comfort for the whole year. Thus, the air conditioners are used to adjust the temperature into the thermal comfort [1]. If the air conditioner is compared to other electrical equipment, is consumes around 50% of the electricity consumption in the whole building [2]. The passive design or design without the energy consumption for the comfort zone would help in the reverse of thinking [3]. One solution to use less energy is to find a suitable way which is good for the environment. Planting trees is another way to help decrease the global temperature. Trees exhale oxygen and absorb carbon monoxide. Therefore, they work as global air filters. If everyone helps grow a tree, we then can have more filters for our planet [4].

From reviewing, it is found that the range of wind speeds for comforting is around 0.25 to 3 m/s and the temperature is in the range of 22-36 degrees celsius. Many types of plants have been studied using the selection criteria to choose a plant for this experiment. One of the contexts in passive design for comfort zone is the attempt to increase the natural ventilation in the building [5]. At the same time, some other green concept would lead to the opposite result of good ventilation. The promotion of having

more plants as green area by growing the plant at the opposite site of patient room can block wind crossing the walk way. The good point is the view of green area but it would also reduce the natural ventilation or block the wind velocity from outside the building. The research therefore investigate the appropriate of bush or garden plant at balcony or the side row of the walk way in front of the patient room in hospital.

Research Objectives

To study the suitable of the garden plant positioning for reduction the wind speed in hospital

Methodology

1.Plant Material

In this study, the *Sansevieria spp*.(Fig1) and *Aechmea fasciata*.(Fig2) was hereby chosen as experimental samples. It is drought resistant plants which is good for the experimant.

Fig. 1 *Sansevieria spp.*

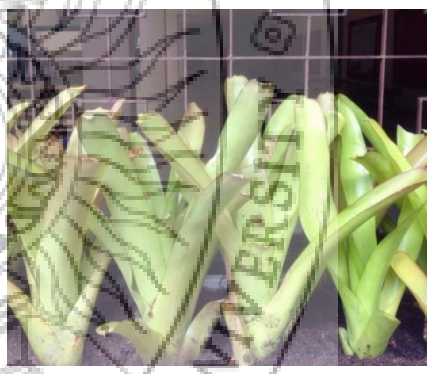

Fig. 2 *Aechmea fasciata*.

2. SITE

The experiment location at the building of the Faculty of Environmental Management, Prince of Songkhla University was sets because inside the building can control the interfere wind speed.

3. Instrument and data collection

The *Sansevieria spp.* and *Aechmea fasciata*.were planted in the prepared plant pots which were categorized at the different heights: 30 cm, 40 cm and 50 cm while being planted as in one row, two rows and two zigzag rows. Each type of the plants was planted based on the set different heights and rows mentioned.

The data collection was the equipment for the measurement of wind speed, temperature and humidity, in a pocket type. The equipment specification was Testo 410-2. A fan which was turned on replacing natural wind was fixed by its speed of 0.5 to 4.00 m/s. The measurement position was at the front of the plants for the building at 0 cm, behind the plants at 0 cm, 50 cm, 100 cm, 150 cm and 200 cm.

Research Results

1. Result from varied wind speed

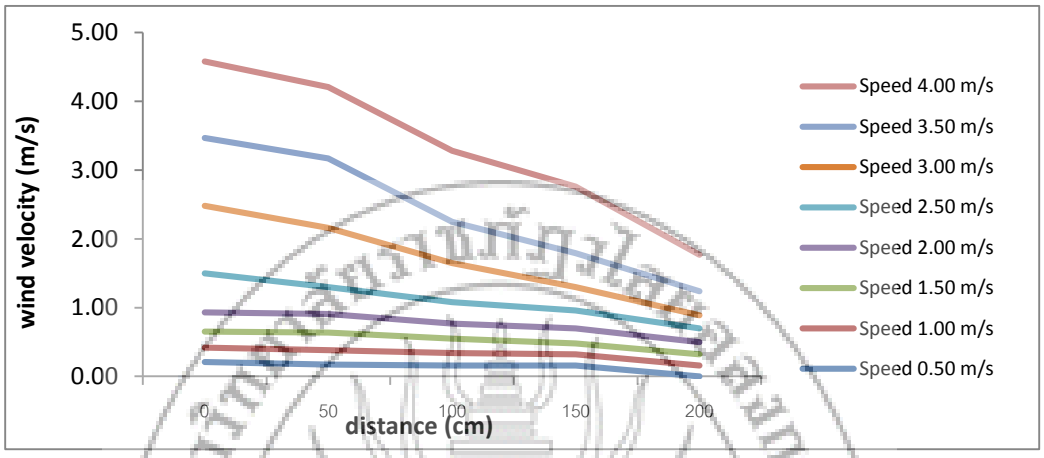

Fig 3 *Sansevieria spp*. at the height of 30 cm, planting 1 row.

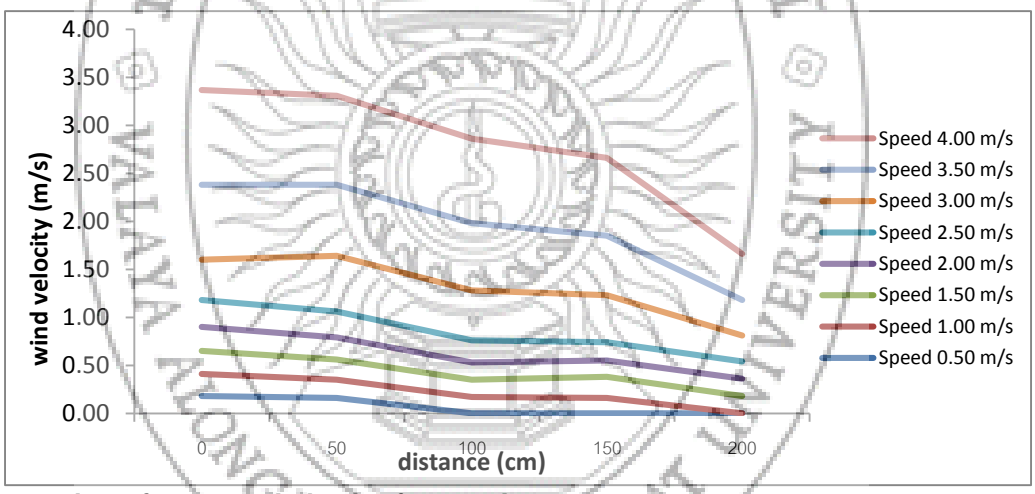

Fig 4 *Aechmea fasciata*. at the height of 30 cm, planting 1 row.

From the experimental results, the flow of wind speed through *Sansevieria spp*. and *Aechmea fasciata*. at the same height and planting layout, in Fig 3 and 4 at the beginning, the wind can flow through the *Sansevieria spp*. better than *Aechmea fasciata*. Therefore, it is concluded that the types of plants affects the wind blow through because of the appearance of leaves and trees.

2. Result at the height of 30, 40, and 50 cm of plant.

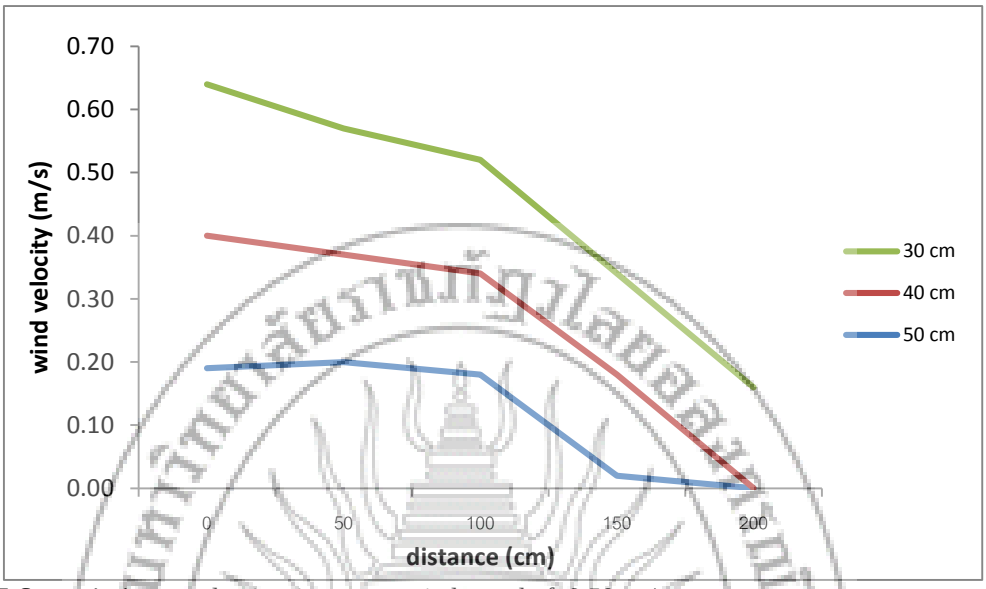

Fig.5 *Sansevieria spp*. planting 1 row at a wind speed of 0.50 m /s.

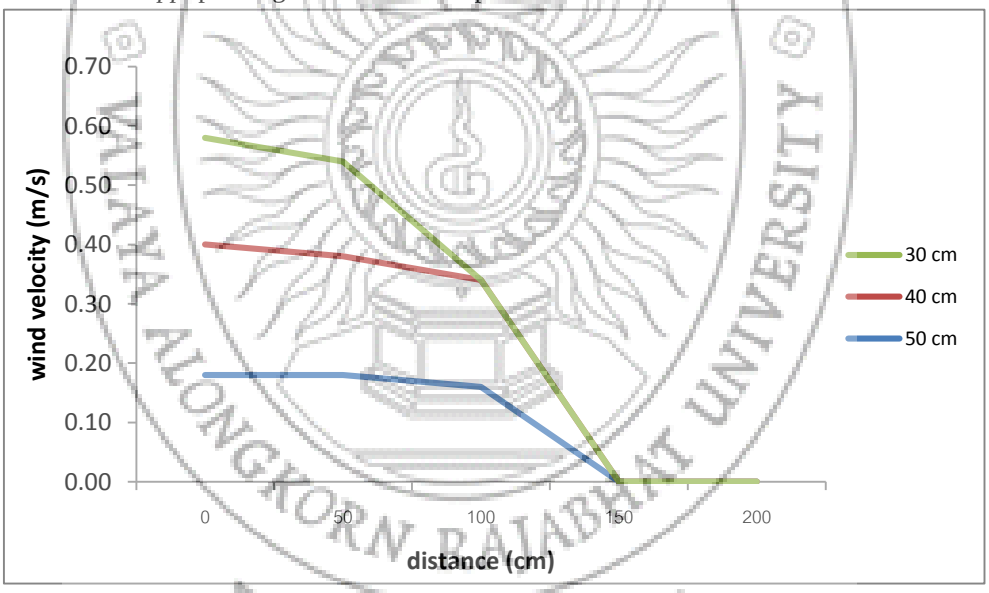

Fig.6 *Aechmea fasciata*. planting 1 row at a wind speed of 0.50 m /s.

From the experiment, when comparing the *Sansevieria spp*. and *Aechmea fasciata*. at different heights as in Fig.5 and 6, it is found that the wind pased the shorter plant better than the higher plant for both *Sansevieria spp* more than *Aechmea fasciata*.

3. Study the layout of planting.

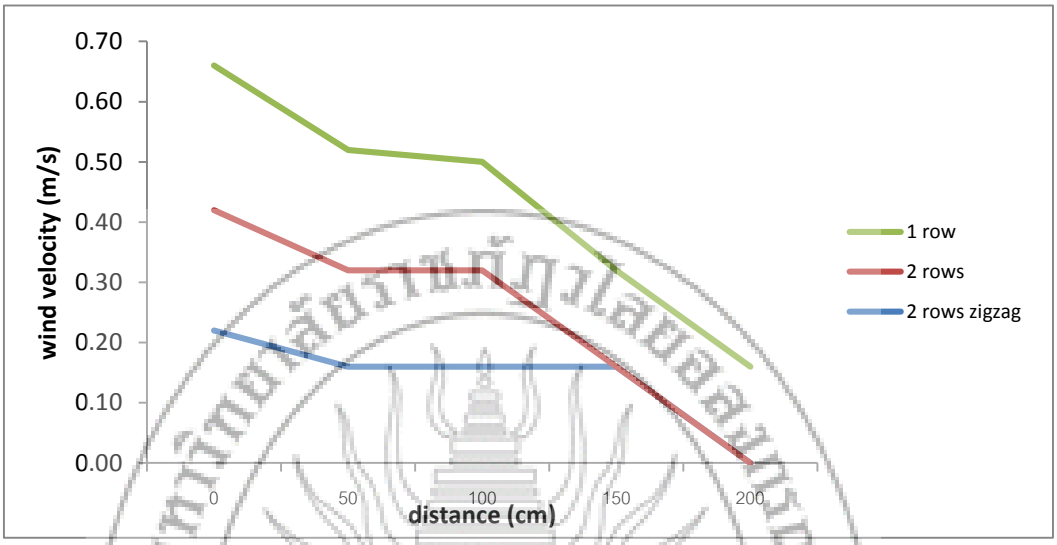

Fig.7 *Sansevieria spp*. at a height of 30 cm, a wind speed of 0.50 m /s

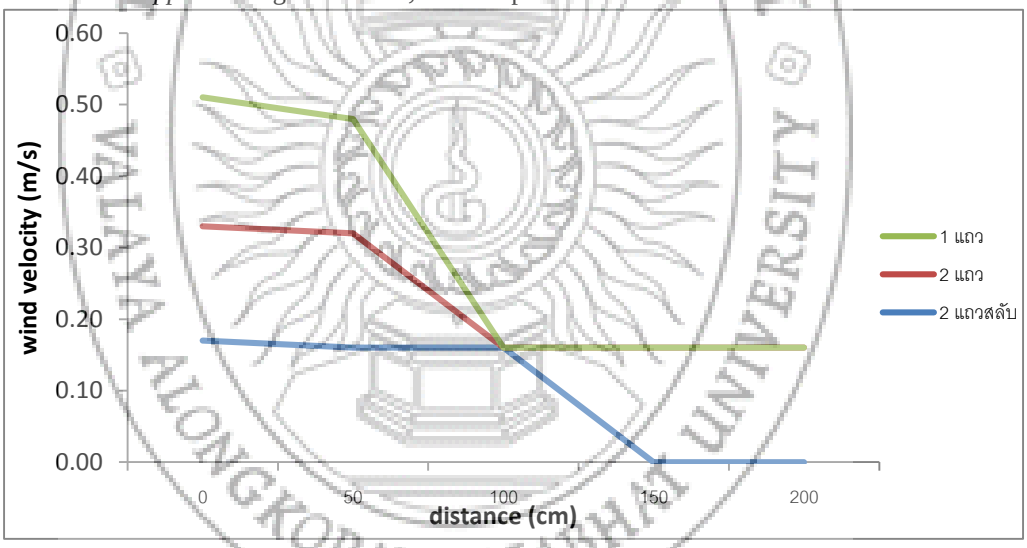

Fig.8 *Aechmea fasciata*. at a height of 30 cm, a wind speed of 0.50 m /s

From Fig 7 and 8, the wind passed through the plant in one row layout better than two rows and two rows zigzag.

Summary and Recommendation

In comparing the two types of plants, it was found that the wind flows through the *Sansevieria spp*. better than *Aechmea fasciata.* In an experiment to the height of plant at 30 cm is better than 40 cm and 50 cm because the higher, the lower of wind speed behind the plant. In the aspect of the plant layout, the one row planting is the best from ventilation compared to two rows and zigzag.

References

Givoni, B. (1998). **Climate consideration in building and urban design.** New York: John Wiley & Sons.

Khedari, J., Yamtraipat, N., Pratintong, N., Hirunlabh, J. (2000). Thailand ventilation comfort chart. **Energy and Buildings.** 32, 245–249.

Auliciems, Andris and V.Szokolay. (1997). **Thermal Comfort. Brisbane**. The University of Queensland Printery.

Chen, J.M., and T.A. Black. (2007). **Defining leaf area index for non-flat leaves.** Plant Cell and Environment. 5, 23-35.

Khedari, J., Yamtraipat, N., Pratintong, N., Hirunlabh, J. (2000). Thailand ventilation comfort chart. **Energy and Buildings.** 32, 245–249.

EFFECT OF SEASONING SYRUP CONTAINING XANTHAN GUM AND SUCROSE ON QUALITY OF DRIED SEASONED SQUID

Duenchay Tunnarut[1] and Rungnaphar Pongsawatmanit[2]

Department of Product Development, Faculty of Agro-Industry, Kasetsart University, 10900, Thailand E-mail: fagiruw@ku.ac.th

ABSTRACT

The amount of seasoning syrup coating on food surface plays an important role for properties of coated product in food industry. In this study, xanthan gum (Xan) and sucrose were used for enhancing viscosity and sweetness of the syrup. A dried squid (1 mm thickness) was used as a food model for coating. The results showed that the viscosity of the syrup increased with increasing Xan and sucrose concentrations leading to pickup enhancement. The syrup containing 55% sucrose showed the highest moisture content and water activity of dried seasoned food model for each Xan concentration. However, the *L** (lightness) decreased with increasing the sucrose content expressed as total soluble solid in the final product. The lower overall liking score of the products found in the samples containing higher syrup pickup was expected from the higher moisture content and sweetness.

Keywords: Xanthan gum, sucrose, properties, syrup pickup, viscosity.

Introduction

Food quality and palatability are important characteristics for product development in food industry. The syrup coating on food surface is usually used for enhancing the taste of the finished product. Sugar is one of the most important ingredients used for enhancing the sweetness and deliciousness of the product (Wang *et al.,* 2014). The amount of seasoning syrup coating on food surface determined by the viscosity plays an important role for properties of coated product. Therefore, the properties of seasoning syrup depend on the ingredients used for syrup preparation. Hydrocolloid is widely used for enhancing the viscosity (Pongsawatmanit *et al.*, 2011) by modifying the rheological properties of the syrup. Xanthan gum (Xan), anionic microbial heteropolysaccharide produced by *Xanthomonas campestris* provides an excellent stability in thermal and acid systems and enhances viscosity stability (Pongsawatmanit *et al.*, 2013). Gabsi et al. (2013) reported that the viscosity of syrup increased with increasing total soluble solids. Therefore, the objectives of this study were to investigate the properties of seasoning syrup containing xanthan gum and sucrose for enhancing viscosity and syrup pickup on the surface of food model. The dried squid with 1 mm thickness was used for syrup coating. Then, the quality of the dried seasoned squid was determined.

Objective

To investigate the properties of seasoning syrup containing xanthan gum and sucrose on surface coating of dried thin squid. The quality of the final dried coated product was also determined.

Materials and methods

Materials

Xanthan gum (Xan) (CP Kelco, San Diego, USA) and commercial sucrose (white sugar) (Mirtphol, Thailand) were used in this study. Maltodextrin with 10-12 DE (Zhucheng Dongxiao Biotechnology Co., Ltd, Dongxiao, China), citric acid (Ajax, Australia), salt, soy sauce, chili powder, monosodium glutamate (MSG) and sodium tripolyphosphate (STPP) were purchased from local market.

Preparation of seasoning syrup and dried seasoned food model

Syrups were prepared from different concentrations of Xan (0, 0.1 and 0.2%) and sucrose (35, 45 and 55%). Each formulation consisting of 5% maltodextrin (10-12DE) and other dry-mix ingredients (7.9%) were mixed with water (about 31.9 – 52.1% depending on the sucrose content in the formulation). The syrup (300 g) was prepared for each formulation. Xan was dispersed in the water and stirred continuously for 30 min with a magnetic stirrer. Then, other dry ingredients were mixed at room temperature for 2 min prior to adding into the Xan dispersion and further mixed for 3 min. The mixture was heated to 72±2ºC and further heated continuously for 1 min before adding soy sauce and chili powder. Then, heating was going on until boiling. Citric acid was added finally after stop heating.

Dried squid (1 mm thickness, 50±2 g) was dipped into the syrup at 55ºC for 2 min. The ratio of dried squid to syrup used was 1:4 (w/w). The excess syrup was allowed to drip off at room temperature for 2 min prior to determine syrup pickup. The coated seasoned food model was dried at 90ºC for 3-5 h to obtain dried seasoned squid with a final moisture content of about 3.2-6.9% depending on Xan concentration, respectively.

Determination of properties of syrup and dried seasoned food model

Steady shear viscosity of syrups containing Xan (0, 0.1 and 0.2%) and sucrose (35, 45 and 55%) were measured using a rheometer (Physica MCR 300, Anton Paar GmbH, Stuttgart, Germany) with the concentric cylinder geometry (CC27) and bottom plate (TEZ150P). All samples (20 ml) were determined at shear rate about 53 s^{-1} at 55ºC. The sample temperature was kept constant at least 5 min before starting measurement.

Syrup pickup refers to the quantity of the syrup adhering to the surface of the dried squid by soaking in the syrup at 55ºC for 2 min and dripping off for 2 min before weighing. The syrup pickup was calculated as the percentage of the syrup weight compared to the initial weight of the dried squid. The measurements were taken in triplicate.

For the dried seasoned squid quality, the moisture content of the food model were determined using a hot air oven (WTB Binder, Tuttlingen, Germany) at 105 °C (modified from AOAC, 2000). The water activity was determined using a water activity instrument (AquaLab Pre; Pullman WA, USA) (modified from Chaethong and Pongsawatmanit, 2015). The total soluble solid was determined using a refractometer (Atago, Japan) by mixing with water before measurement and calculating the value using dilution factor. The color parameter (CIE L^*) was determined using a spectrophotometer (CM-3500d, Minolta, Japan) with a standard illuminant D65, CIE 10° standard observer and 11 mm aperture.

The sensory evaluation of nine dried seasoned squid samples containing different Xan and sucrose contents was performed using 50 untrained panelists recruited from staffs and students of Kasetsart University for acceptance testing. A piece of dried seasoned squid (35 mm x 40 mm x 1.5 mm) was served. Five samples were served in the first session and four samples were served in the second session with 5-min break between the session. Water was provided to the panelists to minimize any residual effect before testing a new sample. Each panel was asked to rate the overall liking of each sample using a 9-point hedonic scale (1 = dislike extremely, 5 = neither dislike nor like and 9 = like extremely).

Statistical analysis

All measurements were performed with at least three replications. The results were reported as the mean value ± standard deviation. The data were subjected to analysis of variance (ANOVA) using the SPSS V.12 statistical software package (SPSS (Thailand) Co., Ltd.). Duncan's multiple range test was also applied to determine significant differences at the 5 % level of significance ($P<0.05$).

Results and discussion

Quality of dried seasoned squid

The viscosity of syrups containing different xanthan gum (0, 0.1 and 0.2%) and sucrose (35, 45 and 55%) contents was investigated at 55ºC and shear rate 53 s^{-1}. The viscosity values of all syrups increased with increasing Xan and sucrose contents, as shown in Fig. 1. The result showed a good agreement with those reported in previous studies of blueberry syrup containing Xan concentration (Pongsawatmanit *et al.*, 2011).

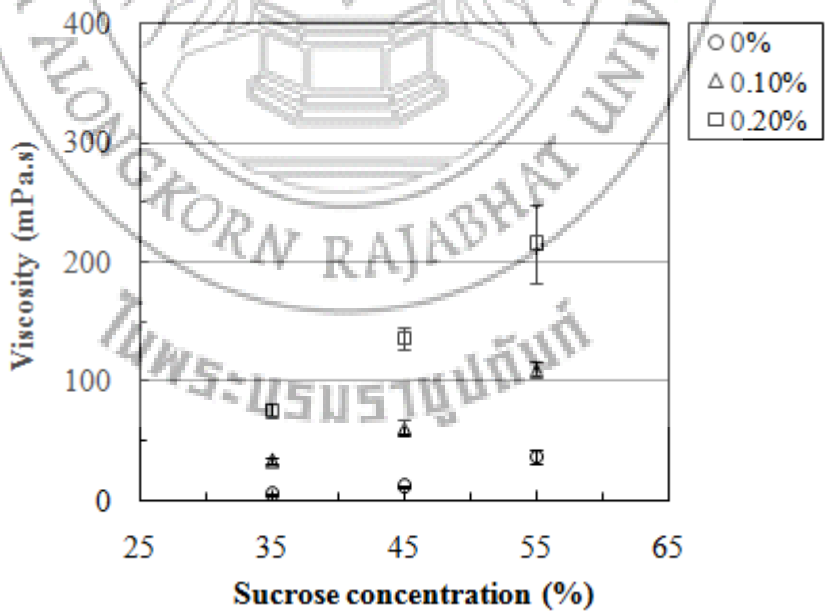

Fig. 1 Viscosity determined at 55ºC and shear rate at 53 $s^{-1}$of syrups containing various concentrations of xanthan gum (0, 0.1 and 0.2%) and sucrose (35, 45 and 55%).

The syrup pickup on the surface of food model increased with increasing sucrose and Xan contents (Fig. 2). The pickup of the syrup containing 0.2%Xan revealed higher than 300% whereas those without Xan exhibited only 154 to 261% of pickup. The results indicated that syrup pickup was enhanced because the viscosity of the syrup increased with increasing Xan and sucrose concentrations.

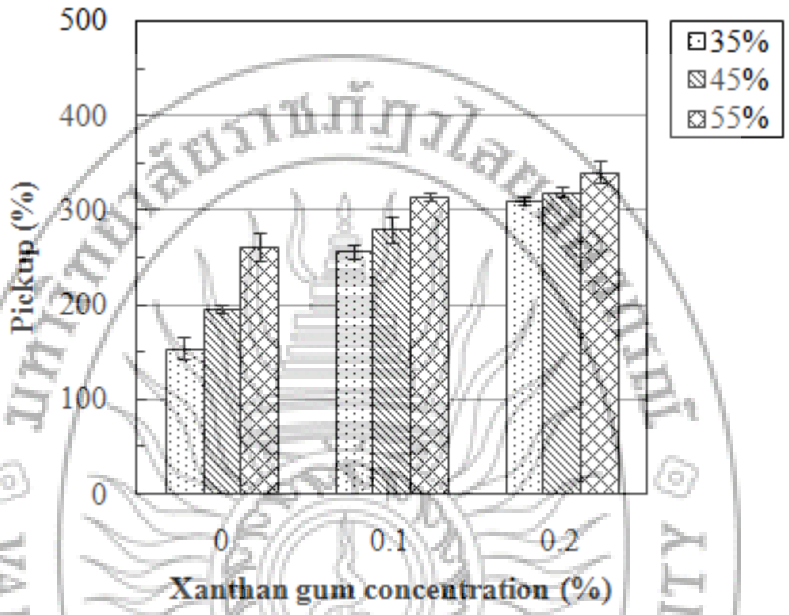

Fig. 2 Syrup pickup of dried squid surface coating using syrups containing xanthan gum (0, 0.1 and 0.2%) and sucrose (35 [⊡], 45 [⧅] and 55 [⧇] %w/w).

The syrup containing 55% sucrose showed the highest moisture content and water activity of dried seasoned food model for each Xan concentration as shown in Fig. 3. The increase in both moisture content and water activity was expected from the higher pickup of syrup and the higher sucrose content in the final dried coated products. However, when surface color was measured, the *L** (lightness) decreased with increasing the sucrose content expressed as total soluble solid in the final product as shown in Fig. 4. The low *L** was observed in the samples (dark browning color) with higher Xan content especially 0.2%Xan due to the syrup pickup >300% and a longer drying time leading to maillard reaction in the final dried food model. The total soluble solid of dried seasoned food model increased with increasing sucrose concentration from 73 to 81 °Brix, 80 to 83 and 81 to 84 °Brix for product containing 0, 0.1 and 0.2% Xan, respectively.

When sensory evaluation was performed, the lower overall liking scores of the products were observed in the samples containing 0.2%Xan (5.6-6.3). The results suggested that the lower overall liking scores in the samples with higher syrup pickup (Fig. 2) enhanced higher sweetness and moisture content leading to the stickiness on the surface of the final dried squid.

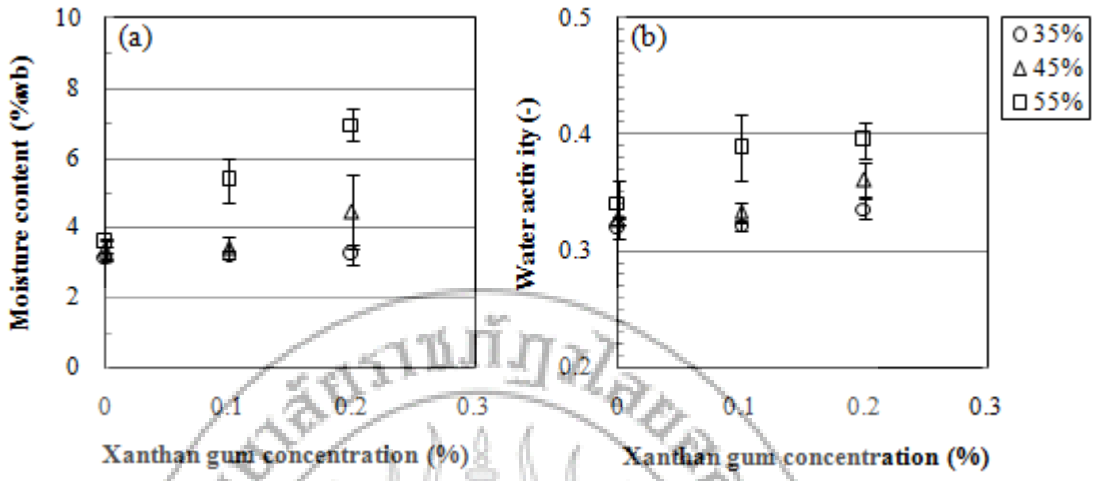

Fig. 3 Moisture content (a) and water activity (b) of dried seasoned squid product as a function of xanthan gum concentrations containing different sucrose concentrations (35 [○], 45 [△] and 55 [□] %w/w).

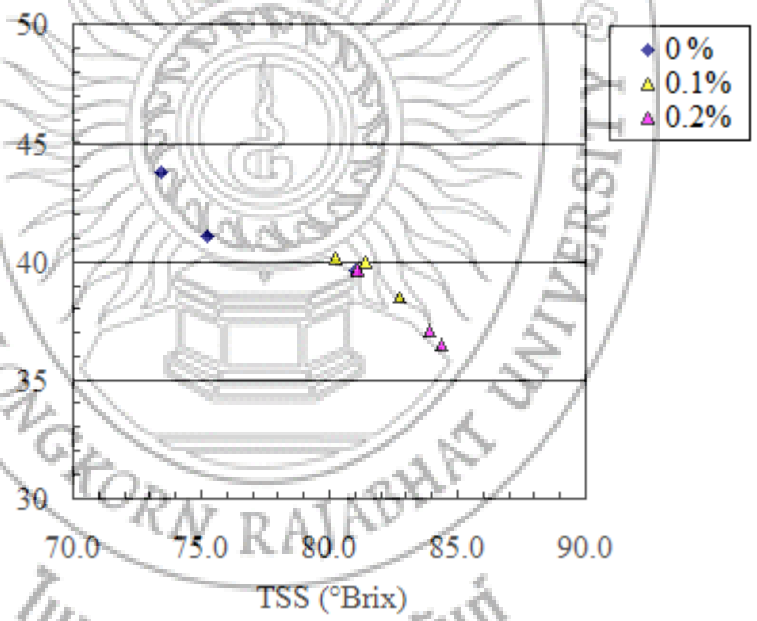

Fig. 4 The *L** parameters as a function of total soluble solid of the dried seasoned squid.

Table 1 The overall liking scores of dried seasoned squid product with different concentrations of xanthan gum (0, 0.1 and 0.2%) and sucrose (35, 45 and 55%).

Xan/Sucrose (%w/w)	Overall liking score
[0/35]	7.4±1.3a
[0/45]	7.3±1.1a
[0/55]	6.7±1.1b
[0.1/35]	5.9±1.6cd
[0.1/45]	6.8±1.5ab
[0.1/55]	5.8±1.4cd
[0.2/35]	5.9±1.5cd
[0.2/45]	6.3±1.5bc
[0.2/55]	5.6±1.7d

*Mean ± standard deviation values (n = 50) of the sensory liking score (1 = dislike extremely and 9 = like extremely) followed by different lower case letters within the same column are significantly different ($p < 0.05$) using Duncan's multiple range test.

Conclusion

The viscosity and pickup of seasoning syrup increased with increasing the concentrations of both xanthan gum and sucrose. The syrup containing 55% sucrose showed the highest moisture content and water activity of final dried seasoned squid. Increased Xan concentration reduced *L** (lightness). The lower overall liking scores of the products were obtained in the samples containing higher syrup pickup due to higher moisture content and sweetness.

Acknowledgements

This study was supported by a grant from the Thailand Research Fund (TRF) under the Research and Researchers for Industries (RRI) project.

References

AOAC. (2000). **Official Methods of Analysis of AOAC International.** 17th ed. The Association of Official Analytical Chemists, Gaithersburg, MD.

Chaethong, K., & Pongsawatmanit, P. (2015). Influence of sodium metabisulfite and citric acid in soaking process after blanching on quality and storage stability of dried chili. **Journal of Food Processing and Preservation**. 39(6), 2161-2170.

Gabsi, K., Trigui, M., Barrington, S., Helal, A. N., & Taherian, A. R. (2013). Evaluation of rheological properties of date syrup. **Journal of Food Engineering**. *117*(1), 165-172.

Pongsawatmanit, R., Chantaro, P. & Nishinari, K. (2013). Thermal and rheological properties of tapioca starch gels with and without xanthan gum under cold storage. **Journal of Food Engineering**. *117*(3), 333-341.

Pongsawatmanit, R., Yakard, N., & Suwonsichon, T. (2011). Effect of xanthan gum on the quality of syrup thickened by modified starch during heating and storage. **Kasetsart Journal (Natural Science).** *45*(1), 128-135.

Wang, Z., Yang, K., Brenner, T., Kikuzaki, H., & Nishinari, K. (2014). The influence of agar gel texture on sucrose release. **Food Hydrocolloids**. *36*, 196-203.

QUALITY OF BATTER AND SPONGE CAKE PREPARED FROM WHEAT FLOUR AND TAPIOCA STARCH USING XANTHAN GUM AS FAT REPLACER

Narida Wiriyakrai and Rungnaphar Pongsawatmanit

Department of Product Development, Faculty of Agro-Industry, Kasetsart University, Bangkok 10900, Thailand Fax: +662-562-5005
E-mail: fagiruw@ku.ac.th

ABSTRACT

The application of hydrocolloid as fat replacer in food product plays an important role in product development. Sponge cake was selected as a food model for creating the food with low energetic value. Flour blend of wheat flour (WF) and tapioca starch (TS) (50/50) was used in this study. Xanthan gum (Xan) (0.1 and 0.2%) acting as fat replacement with butter (0, 8 and 16%) in cake formulation was investigated. The flow behavior of the cake batter revealed non-newtonian fluid ($n<1$). The consistency coefficient (K) of cake batter determined from power law increased with increasing Xan and butter contents. After baking, the quality of sponge cake was evaluated. The water activity and moisture content decreased with increasing Xan and butter contents. Volume index and hardness showed no significance among the cakes with and without butter prepared from 0.1%Xan. An increase in hardness was observed in the cake with increasing Xan content.

Keywords: Xanthan gum, flow behavior, fat replacer, tapioca starch.

Introduction

In the bakery industry, cake is one type of air-leavened product. Cake contains fat, sugar, wheat flour, egg and milk. It is composed of 20-50% fat and 10-30% sugar depending on the types of cakes. The quality of cake depends on many factors such as the ingredients used for batter preparation, aeration of batters and process conditions (Chaiya & Pongsawatmanit, 2011). Wheat flour (WF) is a main ingredient in cake formulation and functions primarily to create crumb structure. However, partial substitution of WF with other flour types [for instance, pea flour (Gomez et al., 2012), tapioca starch (TS) (Chaiya & Pongsawatmanit, 2011)] in cake formulation has been attempted for cost reduction, health reasons or consumer acceptance.

Tapioca starch (TS) is widely used a thickener used in the food industry due to its high viscosity, It is widely used in many products (Pongsawatmanit et al., 2007) because of its low cost, compared to other starches, especially in South-East Asia. Chaiya & Pongsawatmanit (2011) reported that TS could be used for partial replacement of WF for up to 50% in the sponge cake formulation consisting of 20% total flour weight.

Fat replacer using hydrocolloid could be used to produce food products with lower energy intake. Since cakes contain 15 to 25% fat on a batter weight basis. The fat helps in the incorporation of air bubbles into the batter during mixing, assists to leaven the cake product, tenderizes the texture of cake crumb and imparts the moistness (Matsukidou et al., 2010).

Xanthan gum (Xan) is produced by *Xanthomonas campestris*. Xan dispersions show a weak gel behaviour at low shear rates where they reveal a high viscosity (Chantaro et al., 2013); these unique and useful properties make it widely used in food industry. Xan has been incorporated into various products such as rice cake (Turabi et al., 2008) and eggless cake (Ashwini et al., 2009). Therefore, the objective of this study was to determine the quality of cake batter and sponge cake prepared from flour blend of WF and TS (50/50) containing Xan (0.1 and 0.2%) and butter (0, 8 and 16%).

Objectives

The aim of this study was to determine the quality of cake batter and sponge cake prepared from flour blend of WF and TS (50/50) containing 0.1 and 0.2% Xan and butter (0, 8 and 16%).

Materials and methods

Materials

Tapioca starch (TS) was purchased from Siam Modified Starch Co., Ltd. (Pathum Thani, Thailand) with 10.8% moisture content using a hot air oven at 105 °C. Wheat flour (WF) for cake preparation containing 10.9% moisture contents and xanthan gum (Xan) (CP Kelco, San Diego) containing 9.90% moisture content were used for sponge cake formulation. Fresh whole eggs, whole milk powder, baking powder with double-action, emulsifier (SP®), sugar and butter containing 1.5% salt (Orchid®) were purchased from a supermarket.

Sponge cake preparation

Six sponge cake batter formulations from flour blends of WF and TS (mixing ratio = 50/50) containing Xan (0.1 and 0.2%) and butter (0, 8 and 16%) were prepared. The other ingredients consisted of 28% liquid whole eggs, 2% whole milk powder, 24% sugar, 1.6% emulsifier, 0.4% baking powder and water. Cake batter preparation (600 g) was prepared by according to the method of Chaiya & Pongsawatmanit (2011). Each batter formulation (200 g) was placed into an aluminum pan (9 cm x 17.5 cm x 6.5 cm) and baked for 20 min in an electric oven (Teba™, TFL10-31). After baking, the cakes were removed from the pans, cooled upside down on a wire rack for 30 min at room temperature (about 25ºC) and kept in plastic bags to prevent drying.

Determination of cake batter

Flow behavior: The rheological properties of 6 cake batters were determined using a rheometer (Physica MCR 300, Anton Par GmbH, Stuttgart, Germany) with the concentric cylinder geometry (CC27) and measuring cup (C-CC27/T200). Sample temperature was kept constant for at least 5 min before starting measurements. All measurements were carried out at a controlled temperature (25±0.1°C).

The flow behavior of each batter formulation was evaluated using a power law model as shown in Equation (1)

$$\tau = K\dot{\gamma}^{n} \qquad (1)$$

Where τ = shear stress (Pa), $\dot{\gamma}$ = shear rate (s^{-1}), K = consistency coefficient ($Pa.s^n$), and n = flow behavior index. The coefficient of determination (R^2) was also calculated.

Batter density: The batter was filled into an aluminum cup immediately after removal from the mixer. The batter density was calculated as the ratio of the batter weight to the distilled water weight filled in the same cup. The density of the water was 1 g/cm^3.

Determination of sponge cake

Moisture content and water activity of cake crumb was measured using an oven at 105 °C, from 6 to 8 h and a water activity meter (AquaLab Pre, Decagon Devices, Inc., Pullman, WA) at 25 ºC.

Volume index of cake samples were measured by using AACC template method 10-91 (AACC, 1983). In this method, cake is cut vertically through the center and the heights of the cake sample were measured at three different points (B, C, D) along the cross-sectioned cakes using the template. According to this method volume index was determined as shown in Equation (2)

$$\text{Volume index} = B + C + D \qquad (2)$$

Where C is the height of the cake at the center point and B and D are the heights of the cake at the points 2.5 cm away from the center towards the left and right sides of the cake, respectively.

Specific volume and hardness of sponge cake was determined using the rapeseed displacement method and texture profile analysis (TA-500, Lloyd Instruments Ltd., UK), respectively according to the method of Chaiya & Pongsawatmanit (2011).

Statistic analysis

All measurements were performed using three independently prepares samples. The results were reported as the mean value with standard deviation. The data were subjected to analysis of variance (ANOVA) using the SPSS V.12 statistical software package (SPSS (Thailand) Co., Ltd., Bangkok). The significance of differences among means was carried out using Duncan's multiple range test.

Results and discussion

Flow behaviour of cake batters containing Xan (0.1 and 0.2%) and butter (0, 8 and 16%) was evaluated using power law model. The flow behavior of the cake batter revealed non-newtonian fluid (a pseudoplastic behavior with n<1) (Table 1). The consistency coefficient *(K)* of all cake batter determined from power law increased with increasing Xan and butter contents indicating the viscosity of the batter increased with increasing both Xan and butter confirming by Fig. 1. The viscosity of cake batters prepared from flour blends of wheat flour and tapioca starch (=50/50) and different concentrations of xanthan gum and butter was determined at 25 °C and shear rate = 1 s^{-1}.

The batter density is related to the amount of air incorporated in the batter during mixing process leading to determine the expected final baked cake quality. The density of all batters also determined and showed the values of 0.557-0.613 g/cm^3 (Table 1). Batter density (Table 1) showed no significant difference among the different butter contents for both 0.1 and 0.2%Xan.

Table 1 Power law constants, density of batters prepared from flour blends of Wheat flour (WF) and tapioca starch (TS) (WF/TS=50/50) and different of xanthan gum and butter.

Xanthan gum (%)	Butter (%)	Flow behavior			Batter density (g/cm^3)
		K (Pa.s^n)	n (-)	R^2	
0.10	0	14.8±0.8f	0.427a	0.998	0.564±0.012ab
	8	24.3±0.1d	0.400b	0.995	0.560±0.022b
	16	38.5±0.6b	0.389b	0.996	0.557±0.059b
0.20	0	20.2±1.0e	0.315d	0.993	0.613±0.008a
	8	34.7±0.8c	0.338c	0.988	0.613±0.007a
	16	55.5±2.1a	0.276e	0.956	0.601±0.002ab

Mean ± standard deviation values (n=3) followed by a different lower-case letter within the same column are significantly different ($p<0.05$) by Duncan's multiple range test.

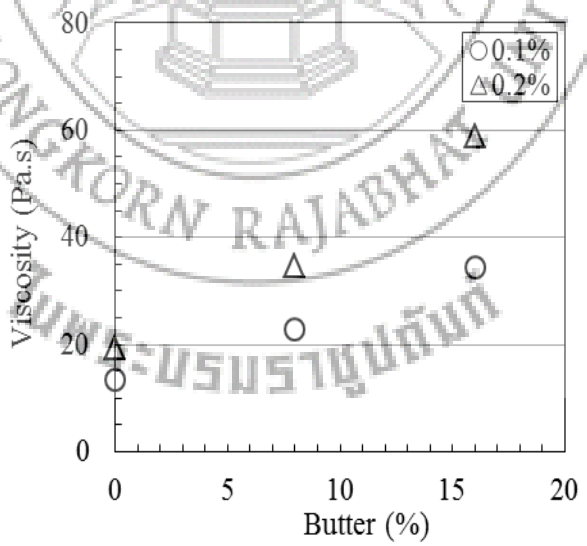

Fig. 1 Viscosity at 25 °C and shear rate = 1 s^{-1} of cake batters prepared from flour blends of wheat flour and tapioca starch (=50/50) and different concentrations of xanthan gum and butter.

After baking at 175°C for 20 min, the quality of sponge cake was evaluated. The water activity and moisture content were determined as shown in Fig. 2. Both water activity and moisture content decreased with increasing Xan and butter contents due to the lower water content in the formulation.

High voluminous cakes are desirable for consumers. The higher volume of cake indicates a higher amount of air remained in the sponge cake during baking process. For the formulations containing 0.1%Xan, the volume index and hardness of baked cakes showed no significant difference among the cake with and without butter (Table 2, $p < 0.05$). However, the volume index and hardness decreased and increased with increasing Xan content. The sponge cake containing 0.2%Xan and lower butter contents (0 and 8%) revealed the lower volume index and higher hardness of the cake (Table 2). We observed a higher volume index value of cakes provided a lower hardness of the cake crumb. Specific volume of cake clearly showed that the values increased with increasing the butter content for each level of 0.1 and 0.2%Xan (Table 2).

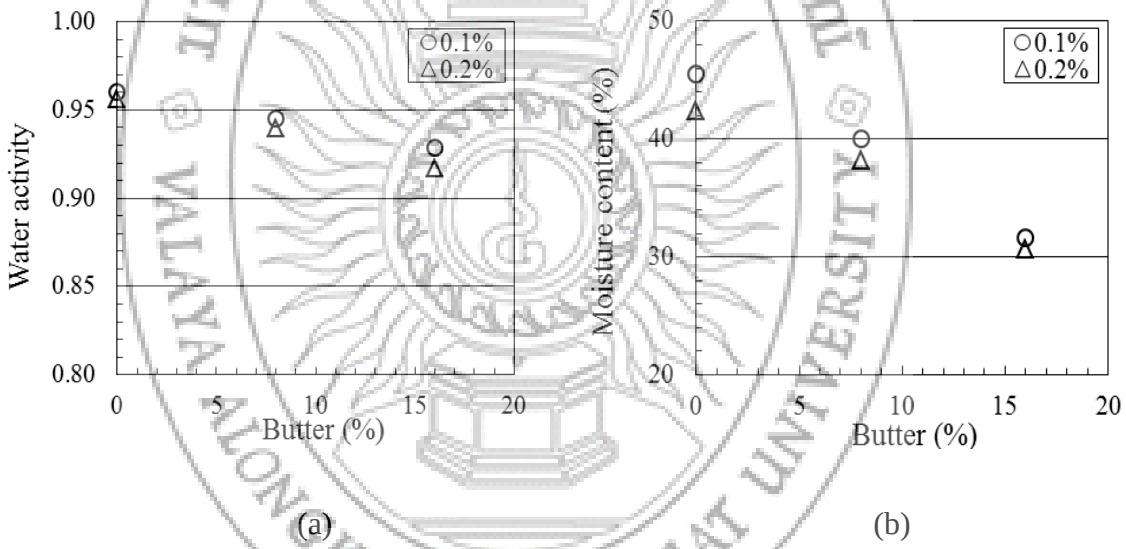

Fig. 2 Water activity (a) and moisture content (b) of sponge cakes containing different concentrations of xanthan gum (0.1 and 0.2%) and butter (0, 8 and 16%).

Conclusion

The viscosity and batter density of the cake batters prepared from flour blend of WF and TS (50/50) increased with increasing Xan acting as fat replacer. Higher water activity and moisture content was observed in the sponge cake with lower butter contents due to the higher water content in the formulation. The Xan (0.1%) could be used to replace the butter for sponge cake preparation.

Acknowledgements

This research was supported by a grant from the Kasetsart University Research and Development Institute (KURDI), Kasetsart University.

Table 2 Volume index, Specific volume and hardness of sponge cakes prepared from different of xanthan gum and butter (WF/TS=50/50)

Xanthan gum (%)	Butter (%)	Volume index (mm)	Specific volume (cm^3/g)	Hardness (N)
0.10	0	126.33±2.31a	4.72±0.10c	2.36±0.17c
	8	127.33±3.06a	5.14±0.06b	1.91±0.23c
	16	128.00±5.57a	6.19±0.07a	2.07±0.45c
0.20	0	117.33±1.53b	4.55±0.17c	5.46±0.96a
	8	119.00±2.65b	6.22±0.09a	4.20±0.31b
	16	127.33±2.08a	6.31±0.07a	3.68±0.56b

Mean ± standard deviation values (n=3) followed by a different lower-case letter within the same column are significantly different ($p<0.05$) by Duncan's multiple range test.

References

AACC (1983). **Approved methods of the AACC. Methods of the AACC, methods 10–91**. St Paul, MN: American Association of Cereal Chemists.

Ashwini, A., Jyotsna, R., & Indrani, D. (2009). Effect of hydrocolloids and emulsifiers on the rheological, microstructural and quality characteristics of eggless cake. **Food Hydrocolloid**. 23, 700-707.

Chaiya, B., & Pongsawatmanit, R. (2011). Quality of batter and sponge cake prepared from wheat-tapioca flour blends. **Kasetsart Journal (Natural Science)**. 45, 305-313.

Chantaro, P., Pongsawatmanit, R., & Nishinari, K. (2013). Effect of heating-cooling on rheological properties of tapioca starch paste with and without xanthan gum. **Food Hydrocolloid**. 31, 183-194.

Gomez, M., Doyague, M. J., & De La Hera, E. (2012). Addition of pin-milled pea flour and air-classified fractions in layer and sponge cakes. **LWT-Food Sci Technol**. 46, 142-147.

Matsakidou, A., Blekas, G., & Paraskevopoulou, A. (2010). Aroma and physical characteristics of cakes prepared by replacing margarine with extra virgin olive oil. **LWT–Food Sci Technol**. 43(6), 949–57.

Pongsawatmanit, R., Temsiripong, T., & Suwonsichon, T. (2007). Thermal and rheological properties of tapioca starch and xyloglucan mixtures in the presence of sucrose. **Food Research International**. 40, 239–248.

Turabi, E., Sumnu, G., & Sahin S. (2008). Rheological properties and quality of rice cakes formulated with different gums and an emulsifier blend. **Food Hydrocolloid.** 22(2), 305–312.

EFFECT OF MECHANICAL PRETREATMENT ON MASS TRANSFER DURING THE OSMOTIC DEHYDRATION OF CHERRY TOMATOES

Pattharasuda Hanucharoenkul[1] and Rungnaphar Pongsawatmanit[2]

Department of Product Development, Faculty of Agro-Industry, Kasetsart University, Bangkok 10900, Thailand E-mail: fagiruw@ku.ac.th

ABSTRACT

Osmotic dehydration (OD) can minimize loss of sensory and retention vitamin in fruit. Mechanical pretreatment using different cutting method was used to determine the suitable process in food industry. Cherry tomato (*Solanum lycopersicum* L.), a climacteric fruit providing sweeter taste than general tomatoes, was selected to investigate the effect of different cutting methods (whole fruit with terminal cutting and half cut fruit) on the OD process. Mass transfer during the osmotic dehydration process at different temperatures (30, 40 and 50 ºC) was evaluated by determining the total soluble solid (TSS) in the fruit. The TSS increased with increasing OD time and temperature. The TSS of half cut fruit was higher than that of whole fruit indicating the mass transfer was improved with the higher values of solid gain and water loss. The kinetic plot of ln k versus $1/T$ of mechanical pretreatment revealed that k values depended on the cutting method. The results gained in this study could be further applied in food industry.

Keywords: Cherry tomato, mass transfer, kinetics, osmotic dehydration**,** pretreatment

Introduction

In Thailand, there are many fruits and vegetables available in the market both in the form of fresh and processed products. Export of fruits and fruit products in 2015 was about 106,184 million baht which increased approximately 10.72% compared to that in 2014 (Office of Agricultural Economics, 2015). Osmotic dehydration (OD) is one popular process to remove moisture (including water activity) in the fruit by immersing fruits in a hypertonic solution leading to an increase in the shelf life or stability of the product. There are two major simultaneous processes occurring in OD: (1) water diffuses from the fruits into the solution and (2) solute transfer from the solution into the fruit tissue. Water removal and solute intake rate during the OD process depend on many factors such as OD temperature and time, mechanical pretreatment (cutting pattern).

Cherry tomato fruit (*Solanum lycopersicum* L. var. cerasiforme) is wild tomato with small and cherry-size (Relf *et al.*, 2016). The tomato was brought into cultivation in Thailand due to it taste sweeter than general tomatoes and popular among consumers. The cherry tomato is found to contain lycopene as an antioxidant and consist of carotenoid pigment that makes red color (Simonne *et al*., 2006). In addition, cherry tomatoes are a good source of lycopene, carotenoids, phenolic acids, ascorbic acid, vitamin E and flavonoids (Karadzhova *et al*., 2015). Heredia and Andres (2008) studied the influence of osmotic solution and temperature on mass transfer phenomena during osmotic dehydration of cherry tomato halves with the aim

of maximizing water loss (WL) and minimizing solute gain (SG). Harati *et al.* (2011) reported an increase in solution concentration resulted in an increase in the ratio of WL to solid uptake. However, previous studies did not study the effect cutting preparation of cherry tomato on mass transfer parameter during OD process using 65 ºBrix sucrose solution. Therefore, in this study, Cherry tomato fruit was selected to investigate the effect of mechanical pretreatment (whole fruit with terminal cutting and half cut fruit) on mass transfer during the OD process at 30, 40 and 50ºC by soaking in 65 ºBrix sucrose solution. The mass transfer was investigated by determining total soluble solid (TSS) and calculating SG and WL during the OD process. The rate constant (*k*) was investigated to find the better cutting method for higher mass transfer of OD cherry tomato.

Materials and methods

Materials

Fresh cherry tomato fruits (*Solanum lycopersicum* L. var. cerasiforme) with light-red stage of maturity were purchased from a wholesale market at Simummuang in Pathumthani Province in September 2016. Sound fruits (2.5 ± 0.3 cm diameter) without physical damage or rotted area were selected, washed, soaked in 0.1% w/w sodium metabisulfite (fruit: solution = 1:3) for 30 min, and kept in refrigeration at 4 ºC. The fruit was used within 2 weeks.

Cherry tomato pretreatment and osmotic dehydration process

The cherry tomatoes were washed and pretreated by soaking in solution containing 0.1% w/w sodium metabisulfite and 2% w/w calcium chloride (fruit:solution = 1:3) at room temperature for 1 h and washed again before cutting as terminal cutting (whole fruit) and half cutting. Both fruit samples were blanched in hot water at 100 ºC for 1 min and drained before OD process.

Half and whole cherry tomatoes were soaked in 65 ºBrix sucrose solution in 350 mL bottle with cap and kept at 30, 40 and 50 ºC. Mass ratio of cherry tomatoes to sucrose solution of 1:2 was used. The fruit samples were taken out from the solution at 0.5, 1.5, 3, 5, 8 and 20 h of immersion, drained and removed the excess of sucrose solution on the surface using absorbent paper. Then, the total soluble solid, weight reduction, water loss and solid gain were investigated.

The osmotic dehydrated half fruit sample were selected to determine the final quality of the dehydrated OD fruit by soaking in 65 ºBrix sucrose solution for 20 h and then blanched in hot water 100 ºC for 3 to 5 sec to remove the syrup on the surface before drying using a tray dryer (BWS-model; Frecon, Bangkok, Thailand) at 70 ºC 2 h and later at 60 °C about 6-8 h until the sample was dried. The moisture content, total soluble solid, pH and water activity were determined.

Mass transfer parameter during osmotic dehydration process

The total soluble solid (TSS) of the fruit was performed. The tomato samples was macerated and a direct measurement was carried out using a refractometer (Atago, Osaka, Japan).

For determining weight reduction, fruit sample during the OD process at selected OD times and temperatures, was taken out. The excess of sucrose solution on

the surface was removed with tissue paper and weighed on a balance. The weight reduction (g/100g) was calculated according to equation (1) (da Costa-Ribeiro *et al*., 2016) as following:

$$\text{Weight reduction (g/100 g)} = \frac{W_1 - W_2}{W_1} \times 100 \quad (1)$$

Where w_1 was the initial weight of the fruit (g) and w_2 was the final weight of osmotic dehydrated sample (g) at selected OD time.

Solid gain (SG) and water loss (WL) were calculated according to equation (2) and (3) (da Costa-Ribeiro *et al*., 2016) as shown below:

$$\text{Solid gain (g/100 g)} = \frac{SS_2 - SS_1}{W_1} \times 100 \quad (2)$$

$$\text{Water loss (g/100 g)} = \left[\frac{(W_1 - W_2) + (SS_2 - SS_1)}{W_1}\right] \times 100 \quad (3)$$

Where SS_1 was the total soluble solid content of sample before osmotic dehydration and SS_2 was the total soluble solid content of osmotic dehydrated sample at selected OD time.

The moisture content of osmotic dehydrated sample was performed using a hot air oven method at 105°C (AOAC, 1995). The water activity was determined with a water activity meter at 25 °C (AquaLab Pre, Decagon Devices, Inc., Pullman, WA) Thailand). The total soluble solid of dried OD fruit was mixed with water and blended before measurement and using dilution faction for calculation. The pH value was measured using pH meter (Cyber scan 510).

Statistical analysis

All measurements were performed at least two replications. The results were reported as mean and standard deviation values. The data were subjected to analysis of variance (ANOVA) using the SPSS V.12 statistical software package (SPSS (Thailand) Co., Ltd., Bangkok, Thailand).

Results and discussion

The mass transfer in osmotic dehydration process

The typical curves of total soluble solid (TSS) for both fruits with terminal cutting (whole fruit) and half cutting as a function of OD time at 30, 40 and 50 ºC in 65 ºBrix sucrose solution is shown in Fig. 1. The TSS values increased with increasing OD time and temperatures. The TSS of half cut fruit was higher than that of whole fruit expected from an increase in surface area of the half cut fruit for mass transfer and the retardation of mass transfer from the skin because the waxy skin of tomato does not allow the mass transfer of water and soluble solids (Heredia and Andres, 2008). The TSS of all syrups used for OD process decreased with increasing OD time and the syrup used for half cut tomato decreased at the larger extent compared with that used for whole fruit (Fig. 1). This confirms that the half cut pretreatment could be used to enhance the mass transfer of the process.

Figure 2 showed the OD time for 20 h. The TSS of the fruit was much higher in the samples done at 50 ºC. The half fruit clearly showed the higher TSS than

those in whole fruit. However, for 20 h of OD process time, we did not observe the equilibrium for both half cut and whole fruit.

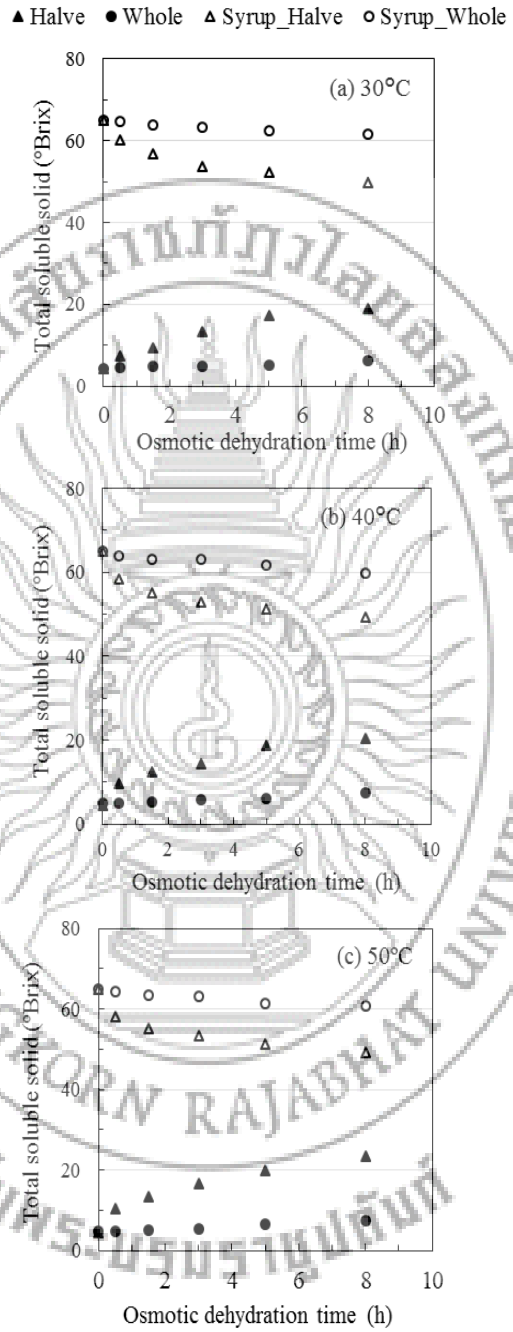

Fig. 1 Total soluble solid of syrup and cherry tomato with terminal cutting (whole fruit) and half cutting as a function of osmotic dehydrated time at 30 (a), 40 (b), and 50ºC (c): The 65 ºBrix sucrose solution used as initial syrup.

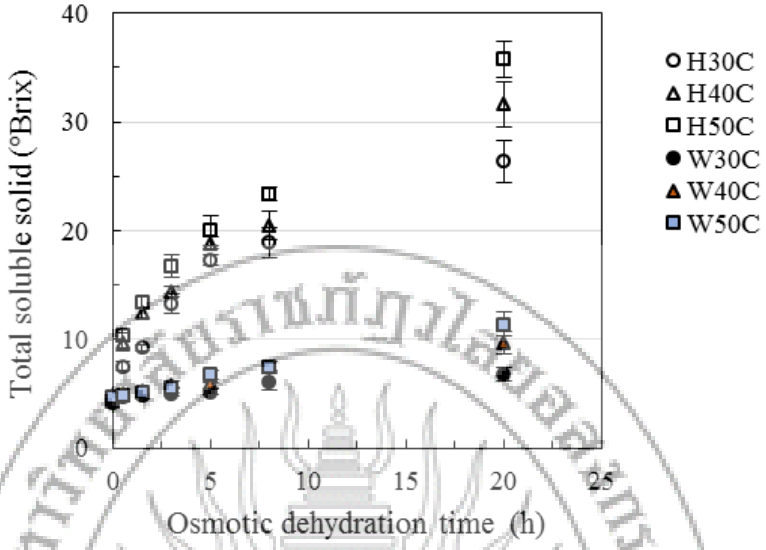

Fig. 2 Total soluble solid of cherry tomatoes with terminal cutting (whole fruit:W) and half cutting (H) as a function of osmotic dehydrated time at 30, 40, and 50ºC using 65 ºBrix sucrose solution.

Weight reduction, water loss and solid gain

The weight reduction (WR), water loss (WL) and solid gain (SG) values of cherry tomatoes with different cutting and OD temperatures were shown in Fig. 3. The results clearly show that mechanical pretreatment with half cutting enhanced the WR, SG and WL values. According to our preliminary test, the WL value calculated from equation (3) was similar to that calculated based on moisture content of initial and OD samples (El-Aouar *et al*., 2006). Half cutting revealed much higher values of WR, WL and SG than those of whole fruit with terminal cutting. Moreover, the WR, WL and SG increased with increasing temperature. The results of temperature effect on WR, WL and SG showed a similar to the previous report of osmotic dehydration of tomato slice (Li *et al*, 2012). Sunjka and Raghavan (2004) also reported that mechanical pretreatment affecting on water transfer by increasing solid gain and moisture loss with quarter's cranberries due to the active surface area enhancing moisture loss and sugar uptake more than cut in halves.

From Fig. 2 at the first 8 h of OD time, the first order kinetic reaction was plotted (data not shown). The rate constant (k) was determined for each OD temperatures for both terminal cutting (whole fruit) and half cutting. Then, the kinetic plot of ln k versus $1/T$ (inverse of absolute temperature) of both mechanical pretreatment as shown in Fig. 4 revealed that k values dependent on the cutting method with r^2 values = 0.879 and 0.935 for half cut and whole fruits, respectively. The results confirmed that half cutting pretreatment could enhance the mass transfer in terms of TSS content in the fruit.

Fig. 3 Weight reduction (a), solid gain (b) and water loss (c) of osmotically dehydrated half cut (H) and whole (W) cherry tomatoes as a function of osmotic dehydration time at 30, 40, and 50ºC using 65 ºBrix sucrose solution**.**

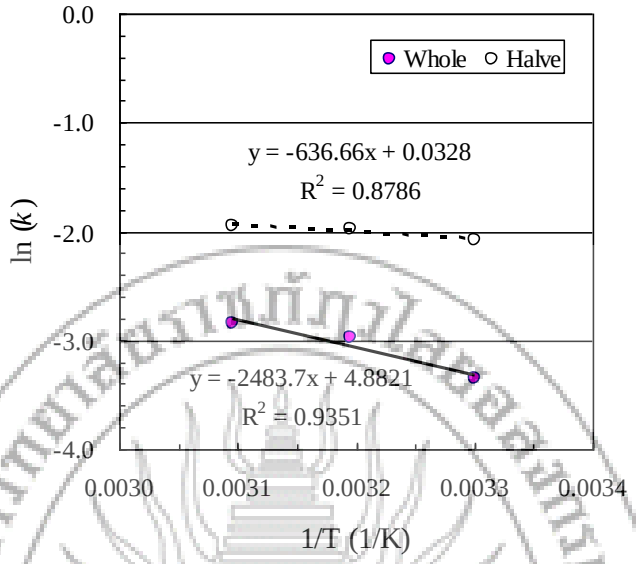

Fig. 4 The plot of ln *k* from the total soluble solid value in tomato fruit versus 1/T (1/K) of osmotic dehydration process.

The osmotic dehydrated half cut fruit sample were selected to determine the final quality of the dehydrated OD fruit by soaking in 65 ºBrix sucrose solution for 20 h because of the higher mass transfer in OD process. The quality of the dried OD fruit is shown in Table 1 with 15.4% moisture content, 0.695 water activity and 71 ºBrix**.**

Table 1 Physical and chemical properties of dried osmotic dehydrated cherry tomato

Physical and chemical properties	**Value**
Moisture content (%, wb)	15.4±0.00
a_w	0.695±0.00
pH	4.47±0.02
Total soluble solid (g/100g)	71.0±4.42

*** Mean ± SD**

Conclusion

The TSS of half cut fruit was higher than that of whole fruit indicating the mass transfer was enhanced confirming by the higher values of solid gain and water loss. The kinetic plot of ln *k* versus 1/*T* of mechanical pretreatment revealed that *k* values dependent on the cutting method. Mechanical pretreatment with half cutting can be used to improve the mass transfer in OD process.

Acknowledgements

This research was supported by a grant from the Kasetsart University Research and Development Institute (KURDI), Kasetsart University.

References

AOAC. (1995). **Approved Methods of the AOAC. Method 925.10(2)**. 16th ed. Washington, D.C: Association of Official Analytical Chemists, Inc.

da Costa Ribeiro, A.S., Aguiar-Oliveira, E., & Maldonado, R.R. (2016). Optimization of osmotic dehydration of pear followed by conventional drying and their sensory quality. **LWT - Food Science and Technology**. *72*, 407-415.

El-Aouar, Â. A., Azoubel, P. M., Barbosa Jr, J. L., & Xidieh Murr, F. E. (2006). Influence of the osmotic agent on the osmotic dehydration of papaya (Carica papaya L.). **Journal of Food Engineering.** *75*(2), 267-274.

Harati, A., Fatemian, H., Hosseini, E., Gh. H. Asadi, Darvish, F. (2011). An Investigation of Mass Transfer Phenomena during Osmotic Dehydration of Orange Slices. **International Journal of Agricultural Science and Research**. *2*(3), 1-10.

Heredia, A., & Andrés, A. (2008). Mathematical Equations to Predict Mass Fluxes and Compositional Changes During Osmotic Dehydration of Cherry Tomato Halves. **Drying Technology**. *26*(7), 873-883.

Karadzhova, K. K., Brashlyanova, B., Yovkova, D. K., & Ivanova, Y. H. (2015). Influences of drying method on cherry tomato Quality characteristics. **Food, Technologies & Health.**

Li, H., Zhao, C., Guo, Y., An, K., Ding, S., & Wang, Z. (2012). Mass transfer evaluation of ultrasonic osmotic dehydration of cherry tomatoes in sucrose and salt solutions. **International Journal of Food Science & Technology**. *47*(5), 954-960.

Office of Agricultural Economics. (2015). **Agricultural Economics Indicators of Thailand 2015.** Bangkok. Agricultural Information Center.

Relf, D., McDaniel, A., & Morse, R. (2016). Tomatoes. **Virginia Cooperative Extension.** Retrieved October 1, 2016, from https://pubs.ext.vt.edu/426/426-418/426-418_pdf.pdf.

Sanjka, P. S., & Raghavan, G. S. V. (2004). Assessment of pretreatment methods and osmotic dehydration for cranberries. **Canadian Biosystems Engineering**. *46*, 3.35-3.40

Simonne, A. H., Behe, B. K., & Marshall, M. M. (2006). Consumers prefer low-priced and high lycopene-content fresh-market tomatoes. **Hort Technology.** *16*, 674-681.

AN INVESTIGATION OF DOWNWARD LONGWAVE RADIATION IN THAILAND

Panatcha Anusasananan[1] Serm Janjai[1] and Itsara Masiri[1].

[1]Laboratory of Tropical Atmospheric Physics, Department of Physics,
Faculty of Science, Silpakorn University, Nakhon Pathom 73000, Thailand. Panatcha02@hotmail.com

ABSTRACT

In this study, downward longwave (LW↓) irradiance was measured at the meterological stations located in four main provinces of Thailand, namely Chiang Mai, Ubon Ratchathani, Nakhon Pathom and Songkhla. To obtain statistics of LW↓ irradiance, LW↓ irradiance data from these four sites were collected and analyzed. Diurnal variations of LW↓ irradiance data were examined. The highest LW↓ irradiance occurred at 14:00-15:00. From seasonal changes, the high LW↓ irradiance period occurred between June-September. Comparisons of LW↓ irradiance derived from all stations with LW↓ irradiance estimated by various models were carried out. It was found that the LW↓ model developed by Sujita and Brutsaert (1998) gave the best agreement to the measurement.

Keywords: Downward longwave radiation, Infared radiation, Thermal radiation

1. Introduction

Downward longwave (LW↓) radiation is an electromagnetic wave radiated by the atmosphere toward the surface of the earth. It is the infrared radiation in the wavelength range of 0.4 to 100 μm with the maximum intensity at about 10 μm. LW↓ radiation is of importance for the energy balance of the earth-atmospheric system (Salby, 1996). LW↓ radiation data are required for accurate atmospheric modeling, which is essential to meteorological and climatological applications. These data are also needed for the analysis of the greenhouse effect in the earth-atmospheric system, helping to understand climate change mechanism (Brindley and Bantges, 2016; Philipona, et al., 2004). The information on LW↓ radiation is usually required for atmospheric research. However, such information is very limited especially in the tropics. In Thailand, LW↓ radiation was first investigated by Exell (1976) using LW↓ irradiation derived from surface temperature. Later, Golaka and Exell (2011) measured LW↓ irradiance at Chiang Rai in northern Thailand and the data from the measurement were analysed. As the information on LW↓ radiation from measurements in Thailand is still limited, we have conducted LW↓ radiation measurements in the North, Northeast, Center and the south of Thailand. The purposes of this paper are to present the variation of LW↓ irradiance from these measurements and to compare the performance of various LW↓ irradiance models with the measurement data.

2. LW↓ irradiance measurements

Measurements of LW↓ irradiance were conducted using pyrgeometers at meteorological stations located in Chiang Mai (18.78 °N, 98.98 °E), Ubon Ratchathani (15.25 °N, 104.87 °E), Nakhon Pathom (13.82 °N, 100.04 °E) and Songkhla (7.20 °N, 100.60 °E) (Figure 1). These stations are located in four main climatic regions of Thailand: a dry northeast (Ubon Ratchathani), a mountainous north with a relatively cool dry season in winter (Chiang Mai), an urban central region (Nakhon Pathom) and a southern equatorial region with no distinct dry season (Songkhla). For each station, a Kipp & Zonen pyrgeometer (model CGR4) was installed on the roof top of the meteorological station building. Voltage and temperature signals of the instrument were recorded using a data logger of Kipp & Zonen (model logbox SD). The voltage and temperature signal were captured every minute and further processed to hourly LW↓ irradiances. The LW↓ irradiance collected from Chiang Mai and Nakhon Pathom were taken during 2011 – 2015 and from Ubon Ratchathani and Songkhla were taken during 2013 – 2015. These data were used in statistical analysis and model comparisons.

Fig. 1 Map of Thailand showing the positions of the LW↓ irradiance measuring stations.

3. Results and discussion

In this study, we examined statistics including diurnal and seasonal variations. The results are summarized in this following sections.

3.1 Diurnal variation of LW↓ irradiance

LW↓ irradiances were averaged for each hour over a period of 5 years (2011-2015) for Chiang Mai and Nakhon Pathom and 3 years (2013-2015) for Ubon Ratchathani and Songkhla. Diurnal curves were obtained for each station and the results were plotted in Figure 2.

Overall, as Ubon Ratchathani and Nakhon Pathom located at about the same latitude band (13°N-15°N) which experienced a similar climate condition, the variations of LW↓ irradiances in Nakhon Pathom and Ubon Ratchathani showed a similar pattern during the days. In contrary, it is very obvious that average LW↓ irradiance at Songkhla station showed the highest values throughout the days. LW↓ irradiances were relatively low at 7:00 – 8:00, then increased to their maximum values at 13:00 – 15:00 and gradually droped again to their lowest in the morning. In addition, Chiang Mai exhibits the lowest LW↓ irradiance compared to the other stations.

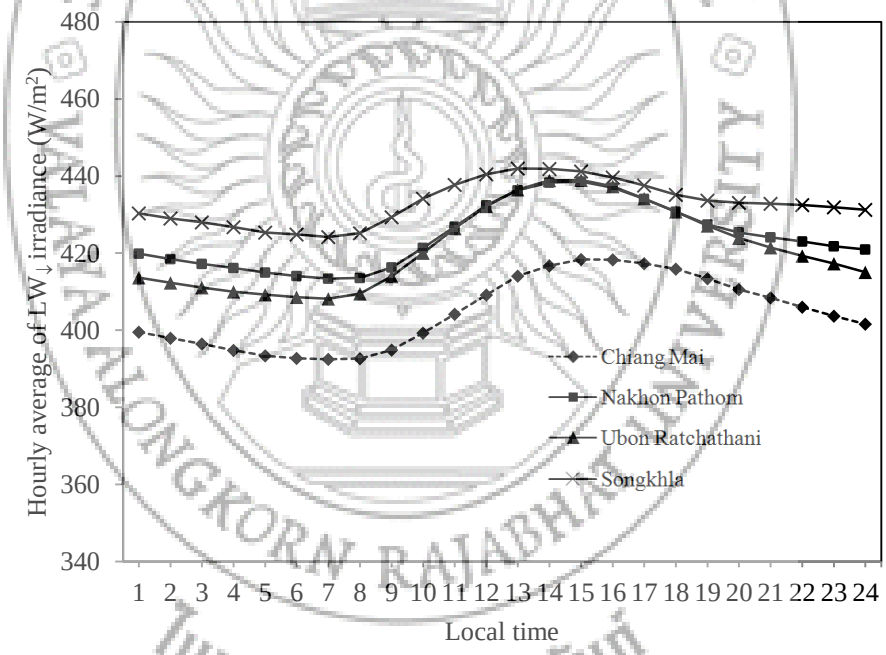

Fig. 2 Long-term hourly average of LW↓ irradiance for the four stations.

3.2 Seasonal variations of LW↓ irradiance

Seasonal variations of daily average LW↓ irradiances are shown in Figure 3. Overall, low values of LW↓ irradiance can be found during winter period except at Songkhla station. By contrast, the highest values of LW↓ irradiance can be observed during wet season from June to October for all stations.

During the dry period (January - March) LW↓ irradiance over Thailand exhibited a pattern of low values ranging between 361 and 393 W/m^2. From May to October, LW↓ irradiances showed the highest values of 430.6 W/m^2, 441.2 W/m^2 and 439.7 W/m^2 at Chiang Mai, Ubon Ratchathani and Nakhon Pathom, respectively. In

November, a sharp decrease of LW↓ irradiance can be observed toward the end of winter period in January. The lowest values of LW↓ irradiance can be seen in January for all stations.

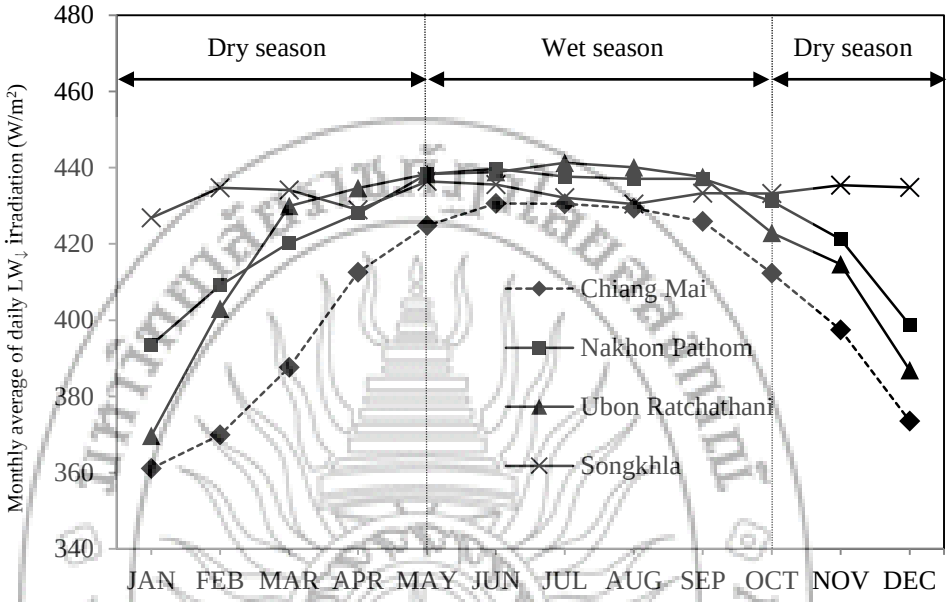

Fig 3. Long-term monthly average of daily LW↓ irradiance for the four stations.

3.3 Comparisons of all-sky LW↓ irradiance models

In order to determine the best performance LW↓ irradiance model for Thailand, we have compared seven all-sky models against the LW↓ irradiance measurement data. In this comparison, a clear sky LW↓ irradiance model developed by Idso (1981) was chosen as a standard clear sky LW↓ irradiance data to the all-sky models. These selected models are written in Table 1.

Table 1. Models used in the comparison. LW_0 irradiance is the LW↓ irradiance under cloudless sky conditions obtained from Idso (1981) and c is the fractional cloud cover.

Author	Model	Coefficients
1. Maykut and Church (1973)	$LW_{\downarrow} = LW_0(1+Ac^{2.75})$	A = 0.22
2. Jacobs (1978)	$LW_{\downarrow} = LW_0(1+Ac)$	A = 0.26
3. Konzelmann et al. (1994)	$LW_{\downarrow} = LW_0(1-c^4)+Ac^4\sigma T_a^4$	A = 0.952
4. Sujita and Brutsaert (1998)	$LW_{\downarrow} = LW_0(1+Ac^{2.45})$	A = 0.049
5.Crawford and Duchon(1999)	$LW_{\downarrow} = LW_0(1-c)+Ac\sigma T_a^4$	A = 1
6. Iziomon et al. (2003)	$LW_{\downarrow} = LW_0(1+Ac^2)$	A = 0.0035
7. Duarte et al. (2006)	$LW_{\downarrow} = LW_0(1-c^{0.671})+Ac^{0.671}\sigma T_a^4$	A = 0.99

The coefficients of the models were also shown in Table 1. The models were used to calculate LW↓ irradiance in 2015 at the four stations. The discrepancies between measured and calculated LW↓ irradiances were presented in terms of root mean square error (RMSE) and mean bias error (MBE) as shown in Table 2. The results showed that the model developed by Sujita and Brutsaert (1998) gave the best performance for Thailand.

Table 2. The performance of the selected all-sky models.

Model	MBD (%)	RMSD (%)	R^2
1. Maykut and Church (1973)	5.58	8.31	0.652
2. Jacobs (1978)	12.23	13.99	0.675
3. Konzelmann et al. (1994)	-0.24	3.00	0.779
4. Sujita and Brutsaert (1998)	**-0.34**	**2.98**	**0.783**
5. Crawford and Duchon (1999)	4.95	6.10	0.767
6. Iziomon et al. (2003)	-2.06	4.10	0.643
7. Duarte et al. (2006)	5.29	6.41	0.735

4. Conclusions

In this study, we have presented statistics of LW↓ irradiance data collected from four stations in the main regions of Thailand. The results obtained from the analysis showed a feature of LW↓ irradiance in Thailand. During the days, LW↓ irradiance was relatively low in early morning and increase to the highest values in the afternoon.

LW↓ irradiance in all three stations at Chiang Mai, Ubon Ratchathani and Nakhon Pathom are low in winter (November to April) with the lowest LW↓ irradiance of 360 W/m^2, 368 W/m^2 and 396 W/m^2 for Chiang Mai, Ubon Ratchathani and Nakhon Pathom, respectively. By contrast, high LW↓ irradiance can be observed in wet season (May to October) as there are more vapor and cloud that effect LW↓ in the atmosphere. On the other hand LW↓ irradiance in Songkhla station showed a different pattern compared to the other stations. Considering all of the stations, the best model for estimating downward longwave radiation was that of Sujita and Brutsaert (1998) with MBD and RMSD of -0.34% and 2.98%, respectively.

5. Acknowledgement

The authors thank Solar Energy Research Laboratory, Silpakorn University for the support of this work.

6. References

Brindley, H. E. & Bantges, R. J. (2016). The Spectral Signature of Recent Climate Change. **Current Climate Change Reports**, 2(3), 112–126.

Crawford, T.M., & Duchon, C.E. (1999). An improved parameterization for estimating effective atmospheric emissivity for use in calculating daytime downwelling long-wave radiation. **Journal of Applied Meteorology,** 38, 474–480.

Duarte, H. F., Dias, N. L., & Maggiotto, S. R. (2006). Assessing daytime downward longwave radiation estimates for clear and cloudy skies in Southern Brazil. **Agricultural and Forest Meteorology.** 139(3), 171-181.

Exell, R. H. B. & Kalwar, M. I. (1976). Atmospheric radiation and sky temperatures in Thailand. **Journal of The Science Society of Thailand**. 2, 160-167.

Golaka, A. & Exell, R. H. B. (2007). Nocturnal downward atmospheric radiation in a tropical wet and dry climate with data from the North of Thailand. **International Journal of Ambient Energy.** 28(2), 73-82.

Idso, S.B. (1981). A set of equations for full spectrum and 8–14 mm and 10.5–12.5 mm thermal radiation from cloudless skies. **Water Resources Research.** 17, 295–304.

Iziomon, M. G., Mayer, H. & Matzarakis, A. (2003). Downward atmospheric Irradiance under clear and cloudy skies : measurement and parameterization. **Journal of Atmospheric and Solar-Terrestrial Physics.** 65, 1107–1116.

Jacobs, J.D. (1978). Radiation climate of Broughton Island, in energy budget studies in relation to fast-ice breakup processes in Davis Strait. **Institute of Arctic and Alpine Research.** 26, 105 – 120.

Konzelmann, T., Vandewal, R.S.W., Greuell, W., Bintanja, Henneken, R., E.A.C. & Abeouchi, A. (1994). Parameterization of global and longwave incoming radiation for the Greenland ice sheet. **Global and Planetary Change,** 9, 143–164.

Maykut, G. A. & Church P. E. (1973). Radiation climate of Barrow, Alaska. 1962-66. **Journal of Applied Meteorology.** 12, 620-628.

Philipona, R., Dürr, B. and Marty, C. (2004). Greenhouse effect and altitude gradients over the Alps – by surface longwave radiation measurements and model calculated LOR. **Theoretical and Applied Climatology,** 77(1), 1–7.

Salby, M. (1996). **Fundamentals of Atmospheric Physics**. Academic Press, New York.

Sugita, M. & Brutsaert, W. (1993). Cloud effect in the estimation of instantaneous downward longwave radiation. **Water Resources Research.** 29, 599 – 605.

THE DEVELOPMENT OF GHANA SEMANTIC TOURISM GUIDE SYSTEM

Theophilus Ayepeh[1] and Jongkol Janruang[2]

Department of Information and Communication Technology
Faculty of Sciences and Liberal Arts
Rajamangala University of Technology Isan
Nakhonratchasima, Thailand
Theophilusayepeh@gmail.com[1], jj@sci.rmuti.ac.th[2]

ABSTRACT

The tourism industry contributes highly to the global economy by creating jobs for individuals. During 2015, the industry's contribution to global GDP is forecast to grow by 3.7% and employment by 2.6%. This demonstrates the sector is enduring ability to generate economic growth and create jobs at a faster rate than any economic sector. Tourism is one of the leading economic sector in Ghana economic growth which create Jobs for Ghanaians. The huge attracted natural and historical places in Ghana is attracting interest from tourist in different countries but the huge and lost data and information about these places sometime cause a lot of stress and time consuming to Tourist who show interest in visiting these site. The aim of this project to develop and implement information system Guide with the help of semantic web and ontology which will help tourist to be spend less time in finding the right information they are searching for. This project is divided into three parts which are the semantic search engine for the Ghana information system Guide and the creation of Ghana tourism Ontology and also the information system Guide. The main focus this paper will be on the semantic search engine with help of Ontology as the knowledgebase. The search engine uses ontology and the verbs words to expand user keywords and then Google Custom Search API will be used as a tool for retrieving information related to those keywords. The whole system was evaluated by users and used usability testing method which has two phases, first phase is the test phase and the second phase is the explain the data receive from users in the test phase. The result of the evaluation prove that our system can help user perform their tasks easily and get the right information they are looking for, and also help user to spend less time in searching for information about Ghana tourism industry.

Keywords: Ontology, semantic search, Google Custom Search API, Information system.

Introduction

Currently, tourists use internet to search for travel relevant information. However, they experience an information overload and time-consuming. It is also a difficult job for them to select relevant and appropriate travel data according to their interests, which has affected the tourism industry in Ghana since the tourist across the globe does not found relevant information about tourist places in Ghana. The information about historical event, historical place and other attracted places that tourist would like to visit is not enough on the web to convince tourist and visitors to plan a tour to these places. Some of these systems has search engine problems since the semantic of the user query is not considered and solely based on the keyword. This makes user query meaningless

sometimes and produce irrelevant result. Ghana has a lot of tourist attracted places all over the country but user find it difficult to search for this rich tourist places on the search engines such as (Google, yahoo and many more) to get the relevant information they are looking for. The user may not have enough time to search separate hyperlinks that are generation in the traditional web and causes the user to stop planning for the trip to the country. This problem is not helping the tourism industry in Ghana to grow. This is some of the related works in the tourism ontology and semantic tourism search. Searching tourism information by traditional search engines based on keywords is becoming more difficult and time-consuming [1]. Since it is based on keyword and has no semantical understanding both to the machine and human which provide user with irrelevant information. Often the keyword based search engine do not provide the accurate result as it cannot find the meaning of the user query to the expression used in the web pages.

The literature [2] introduces an application developed with Ontology **search engine** for Agricultural based on FAO Agrovoc Ontology and Google API. They stated that the FAO Agrovoc Ontology is not only an agricultural concepts collection but also the relationships among the concepts, Google API can be used to submit keywords to Google search engine and get the retrieval results from Google, the combination of these two things can help users in agriculture field find information they want to search better and navigate the knowledge in some degree.

The literature introduces the development of tourism ontology, there are several tourism ontologies that has been already developed. These are HarmoNET Ontology [3] which focuses specifically on the following four sub-domains (Events, Accommodation, Attractions, Food and Drink) and the e-Tourism Ontology [4] which focused on (accommodation and activities) including also the necessary infrastructure for the activities. QALL-ME ontology [5] is the most advance and complete tourism ontology. It covers several important aspects of the tourism industry, including touristic destinations (i.e. cities and towns), sites (i.e. accommodation, gastro, attraction, and infrastructure), events (e.g. movie and show) and transportation. The main purpose of the ontology was to provide a common vocabulary for the selected domain and a computerized specification of the meaning of terms used in the vocabulary. The literature [6] developed a semantic information retrieval using ontology in university domain which design, develop and implement a semantic search engine- SIEU (Semantic Information Extraction in University Domain) confined to the university domain. SIEU uses ontology as a knowledge base for the information retrieval process and it is not just a mere keyword search. It is one layer above what Google or any other search engines retrieve by analyzing just the keywords. The developed system retrieves the web results more relevant to the user query through keyword expansion. The overview of the literature gives different approach in semantic information retrieval and the weakness of traditional search engine and also the creation of tourism Ontology. In this proposed system, in combination with some of the above said methodologies, some more procedures have also been added to perform tourism semantic information extraction in a better way.

A. SEMANTIC WEB

The Semantic Web is a Web with a meaning. It describes things in a way that computers can understand. It is an extension to the normal Web and is not about links -relationships between things and its properties. Conventional Web consists of human operator and uses computer systems for tasks like finding, searching and aggregating whereas Semantic Web is the one understood by computers, does the searching, aggregating and combining information without a human operator. It is easily process able by machines, on a global scale. It is the efficient way of representing data on the World Wide Web.

B. SEMANTIC SEARCH

Semantic search seeks to improve search accuracy by understanding the searcher's intent and the contextual meaning of terms as they appear in the searchable dataspace, whether on the Web or within a closed system, to generate more relevant results. Semantic search systems consider various points including context of search, location, intent, variation of words, synonyms, generalized and specialized queries, concept matching and natural language queries to provide relevant search results [7]. Semantic search lends itself well with this approach that is closely related with exploratory search. Rather than using ranking algorithms such as Google's PageRank to predict relevancy, semantic search uses semantics, to produce highly relevant search results. In most cases, the goal is to deliver the information queried by a user rather than have a user sort through a list of loosely related keyword results [8]. Seth Grimes lists "11 approaches that join semantics to search", and Hildebrand et al. provide an overview that lists semantic search systems and identifies other uses of semantics in the search process [9].

C. Ontology

An ontology is a specification of a conceptualization [10]. There are two important points in the definition, first the conceptualization is formal and hence permits reasoning by a computer second ontology are designed for some particular domain of interest [11]. Ontologies describe vocabularies as a kind of complex (meta-) data schemata that are used in order to combine semantic metadata and offer added-value services on top of semantic descriptions. Concepts and relationships are basic components in an ontology. Information integration from different sources needs to be a shared by understanding of the relevant domain. Ontologies provide a common vocabulary to support sharing and reuse of knowledge. Ontology is a fundamental component for achieving the Semantic Web. Ontology has the capability to solve a number of problems in tourism.

D. Google Custom Search API

The Google Custom Search API is a library in different programming languages such as (JavaScript, java) that allows one to embed Google Search in one’s web pages and other web applications. The API exposes a raw Restful interface that returns JSON encoded results that are easily processed by most languages and runtimes. With Google Custom Search API, an application can search the giant Google information store very easy, just send a keyword to the API, and then the results will be feed back to the application which load the API [12].

Research Objectives

At a theoretical level, the research tries to emphasize a complete understanding from Ghana tourism perspective of the problem occurring in the Ghana tourism with a novel approach to address how to help solve these problems associated with Ghana tourism Domain. At a physical level, the research investigates state of-the-art tools, development techniques, applications, standards, limitations, and likely future trends associated with the Semantic Web in tourism information Guide system and its application to tourism industry in Ghana. The main aim of this research are to:

1. Providing deep insight about the problems occurring in Ghana tourism domain
2. Developing semantic search engine for the tourism information Guide system.
3. Develop more understandable information system of Ghana tourism domain on the Web which can be more semantical to both humans and machine.
4. Developing semantic search engine for the tourism information Guide system.
5. Reusing an existing tourism Ontology model to create new tourism Ontology to Ghana Tourism.
6. Evaluate the system by Users

Methodology

In this project we focused on adding semantic web to tourism information system Guide to make user get meaningful result. The project is divided into four parts which are as follows:

- Ghana Tourism Semantic Search engine
- Tourism Ontology Construction
- Ghana Tourism Information Guide System.
- Evaluation of The System by Users Method

The Ghana Tourism semantic search engine is embedded in the Ghana Tourism Information Guide system. The tourism ontology serves as the knowledgebase which helps to expand the user keywords. The Ghana Tourism Information Guide System carries all the information's about Ghana Tourism domain from different source which all combine in one platform.

The following below show the step by step method and technique of the project.

1. Ghana Tourism Semantic Search engine

The architecture overview of the Search engine starts with the user query which query into the search engine and then extract the sentence into relevant words. The relevant words are being represented as list of words which is being compared with the ontology which is the knowledgebase to find the semantic related words that match the list of

query words. The semantic related words are being sent to the google search Api to retrieve the relevant information to the User.

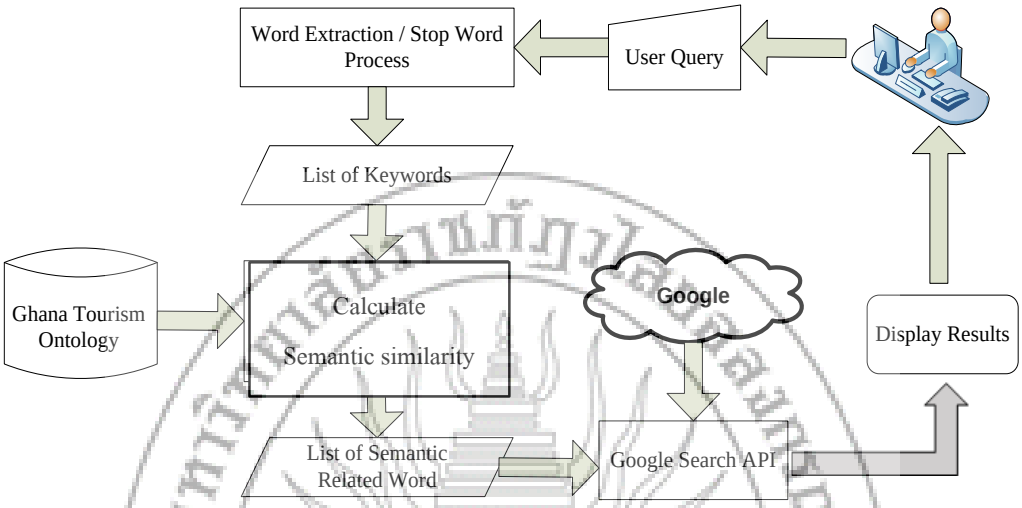

Fig 1. The principle of the search engine called semantic search engine for Ghana tourism domain with
Ontology

The five process of the semantic engine for Ghana tourism domain are explain in detail below:

1.1.User query

The user query is where the user input keyword or sentence which is then submitted to the search engine process to retrieve the right the information as the query result.

1.2. Word Extraction Process

The word extraction uses the stopword and stemming word to extract words or sentence into it meaningful part and then compared with the ontology to find their semantic similarity. Example is shown in Fig.3 and Fig.4

1.3. Semantic similarity

In the semantic similarity we use our concept to create our own algorithm to prove the semantic relation. The fig below illustrates the whole process of our semantic similarity algorithm.

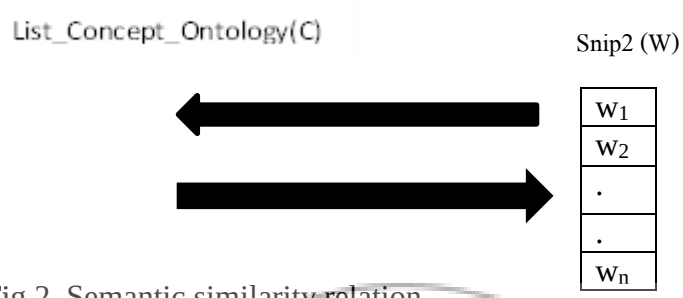

Fig.2. Semantic similarity relation

Snip2 is the list of words which we defined as **W.**
List of concept Ontology which we defined as **C.**
The **W** is the list of words derived from the query.
The semantic related words are represented as **S.**

ALGORITHM

$C = \{c_1, c_2, \ldots, c_n\}$

$W = \{w_1, w_2, \ldots, w_n\}$

S= null

For i =1 to n do {

For example:
C= {labadi beach, la palm hotel, Accra Cultural center, located}
W= {labadi, beach, located}
That means *labadi* is w_1 and it is semantically related to *labadi beach* which is the C_1
Also, beach is w_2 and it is also semantically related to *labadi beach* which is the C_1
Located is w_3 and is related to C_4
Thus, c_4 is added with c_1 and then added to S.

1.4. Semantic related word

The system gets the result of both list of words and ontology after the semantic similarity process is being perform on both. This result is the precise vocabulary which describe the concepts that user want to retrieve, and then submit the right vocabulary to Google through google custom search API.

C_1
C_2
.
.
C_n

1.5. Google custom Search API

The system submits the right vocabulary or vocabularies to the google custom search API which retrieve the right information such as (web link, snippet, title) to the User.

1.6. Display Result

The result retrieve from google is being display to the User using both the JSP and HTML code.

2. Tourism Ontology Construction

This component describes the construction of ontology which forms the knowledge base of this tourism search engine. The concept of this tourism domain is gathered from several tourism ontologies such as (QALL-ME Ontology, HarmoNET ontology and e-tourism Ontology) and from other Ghana tourism website. These concepts are clustered in a hierarchical form in ontology which serves as database for the keywords related to Ghana Tourism domain. The system searches the Ghana tourism ontology base to find the concepts that match the keywords input by user, if the keywords input is a sentence, the system will divide the sentence and find the core words of the sentence and use these words to retrieve the Ghana tourism Ontology Base. Example of Ghana tourism Ontology as shown in Fig. 3

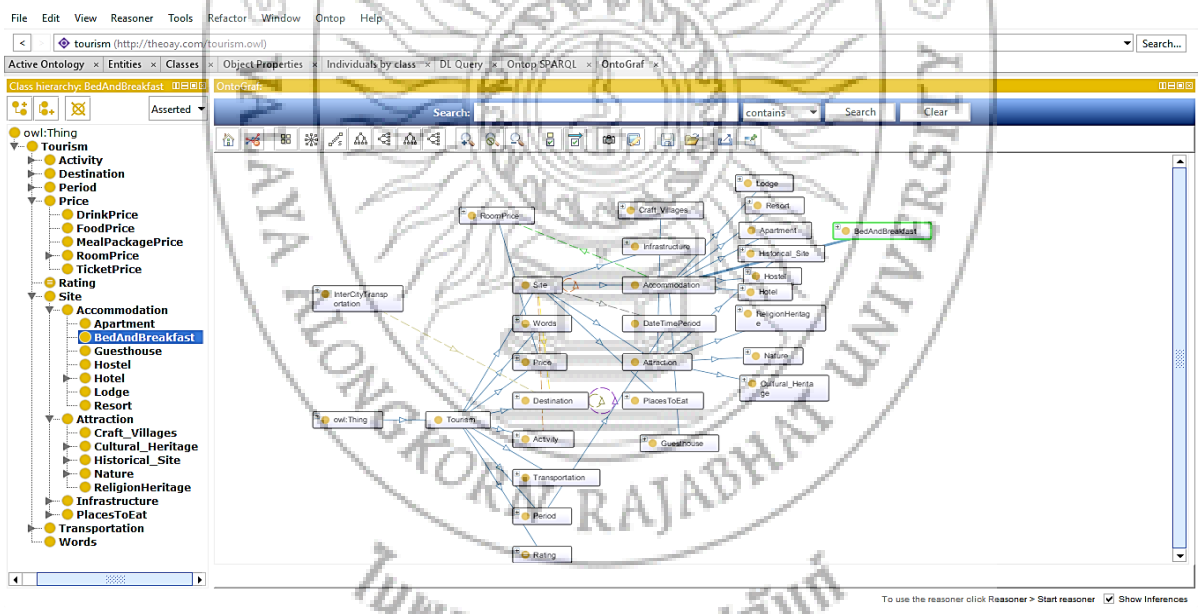

Fig. 3 represent the structure of Ghana tourism ontology using protégé

3. Ghana Tourism Information Guide System.

Tourism is a vital industry to the economies of most countries worldwide (developed or less developed). It represents a cross-sectoral industry, including many related economic sectors such as culture, sport or agriculture, where over 30 different industrial components have been identified that serve travelers (Werthner 2003, p. 1). The components include services such as accommodation, car hire, air travel, and guided tour. The Ghana Tourism Information system is a system that consist of all the necessary information from Ghana tourism domain with it locations and provide services such as hotel booking and attracted

places booking. The main concept is to help users to find the appropriate information they are looking for without wasting of time.

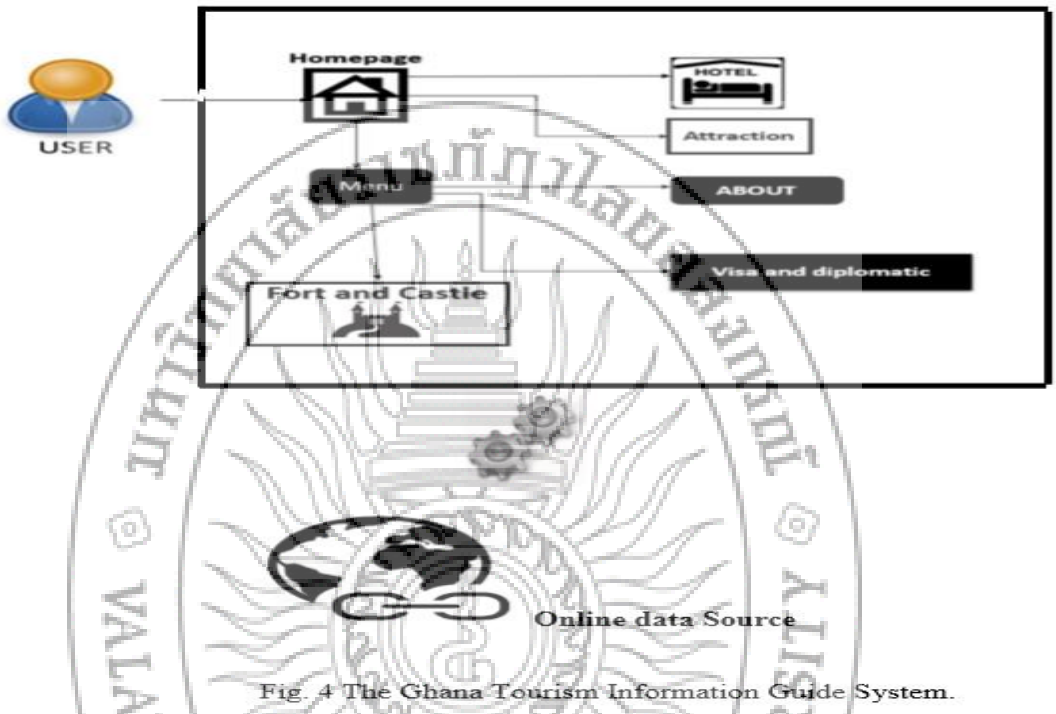

Fig. 4 The Ghana Tourism Information Guide System.

4. Evaluation of The System by Users Method

In our evaluation of the system we used a proposed usability testing method by Ebitisam K. Elberkawi[14] which was uses a summative usability testing plan. The testing used is a performance measurement. Summative usability testing is the summative evaluation of a product with representation users and tasks designed to measure the usability (defined as effectiveness, efficiency and satisfaction) of the complete product. The proposed techniques were proposed by them which is to obtain quantitative data about test participants performance, when they performed the task during the usability test. The test was conducted in Rajamangala University computer laboratory with five participants being used as users to collect accurate data from them. The participant was given a pre-test training and a list of prepared task was provided to users. The aim for the usability testing in terms of usability attribute (eg. Easy to learn, efficient to use, easy to remember, few errors, subjectively pleasing) has been defined. The usability issues were to determine by measurement such as:

- The time user takes to finished a specific task.
- The time spent recovering from errors.
- The number of user errors

The method is based on two factors: Tasks and Time. The system is being divided into subparts to be evaluated, each of which is called a Task. The task is being divided into two parts which are the Page task and Task Question. The time is an important factor

which helps to criticize the system since one of our main aim of this system is to help users to be less time consuming when search for information. The method is divided into two phase. The phase one which consist of the Test plan, Role (eg. Participant, Facilitator and observer), Training and sessions, Metrics. The result of the first phase are assembled as showed in Table 1. The Usability measures are related to the factors of tasks and times, as follows:

- The time X: $X_n > 0$ (in minutes) that users take to complete a specific task called "Total Task Time "
- The time Z: $Z_n >= 0$ (in minutes) that is spent in recovering of mistakes called "Mistake Time" where $X_n >= Z_n$
- The number of user mistakes Y: $Y_n >= 0$ is called "Total Task Mistakes"

Table I General Design of Testing Table

Page Task	Task Question(TQ)	Total Task Time(min)	Total Task Mistakes(min)	Mistake Time (min)
Page 1 Task	TQ1	X_1	Y_1	Z_1
Page 2 Task	TQ2	X_2	Y_2	Z_2
Page 3 Task	TQ3	X_3	Y_3	Z_3
Page 4 Task	TQ4	X_4	Y_4	Z_4
Page 5 Task	TQ5	----------	----------	----------
Page 6 Task	TQ6	X_n	Y_n	Z_n

The second phase present the collected data in two charts. The first chart uses the data from the total task mistakes whiles the second chart uses the data from overall time and time of mistakes.

Research Results

The results of the experiment use the knowledgebase of Accra tourism domain in the Ghana tourism Ontology we created from the other ontologies which is

A. RESULTS OBTAINED IN EVERY LEVEL IN THE SEMANTIC SEARCH ENGINE:

The Ghana Tourism semantic search engine helps the users to get the right information they are searching on the web with the help Accra tourism domain in the Ghana tourism Ontology which serve as the knowledgebase to the system.

The following below shows the step by step process of how the search engine retrieved appropriate result.

- **SAMPLE QUERY ENTERED BY THE USER:**
  The user enters the information into the search interface. Example is in Fig4 (Where is labadi beach located?)

Fig.5. User Query into the Search Engine

- **Filtering and Parsing the Input of the Query**
  From the Fig4 User query is being filtered by extracting algorithm which filter out the words and parse the query and as shown in Fig5.

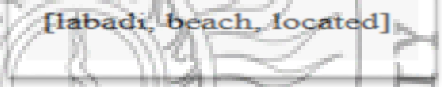

Fig.6 List of words

- **EXTRACTION OF DOMAIN KEYWORDS FROM ONTOLOGY:**
  The domain keywords which are semantically related to the words in the Fig6 are extracted from ontology and as shown in Fig7

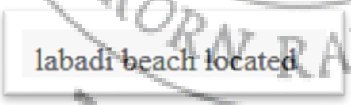

Fig.7. semantic related words

- ***WEB LINKS RETRIEVED:***
  After the User entered the query our proposed system processed the query into different steps which is shown in Fig.6 and Fig7 before it retrieved the web links from Google and it is shown in Fig8.

Fig.8. The appropriate link of the User query result.

- ***DISPLAY RESULT***

After the User clicked on the first link from Fig8 it displayed the location the user is looking for which is shown in Fig9.

Fig9. The result of the first link from our proposed system

B. RESULTS OBTAINED IN THE GHANA TOURISM INFORMATION GUIDE SYSTEM:

i) The overview of the system results from all the pages

Fig.10 shows the Attraction Page

Fig. shows the homepage of Ghana Tourism Information Guide System

Fig 12. shows the menu in the homepage

The fig.11 shows the Hotels Page

The fig.13 shows the Visa and diplomatic Page

Fig 14 shows the About Ghana Page

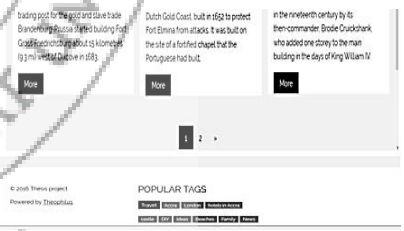

The fig.15 shows the Fort and Castle Page

ii) Example of User Question results in the Tourism Information Guide System

I. The User

The user is looking for the answer to the question below.
Question: Where is labadi beach located and it nearby hotels

II. Display User result

The result of labadi beach in the Attraction Page has three important things such as (history about labadi beach, location of labadi beach, nearby hotels

The fig.16 shows the Attraction of beach section

The result of the History is in Wikipedia. The fig.16 below shows the result

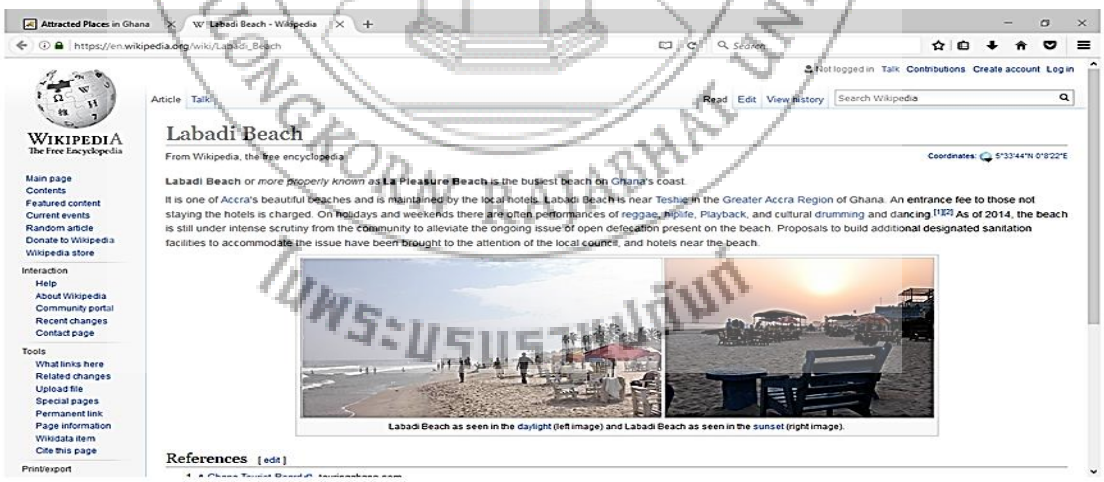

The fig.17 shows the history of labadi beach from Wikipedia

The result of the labadi beach location is in the fig.20 below.

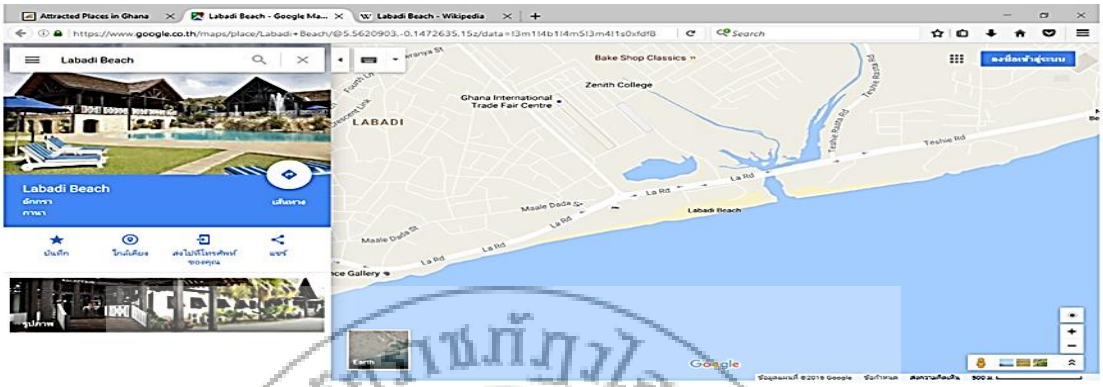

The fig.18 shows the google location of labadi beach

The result of the labadi beach nearby hotels is in the fig.19 below.

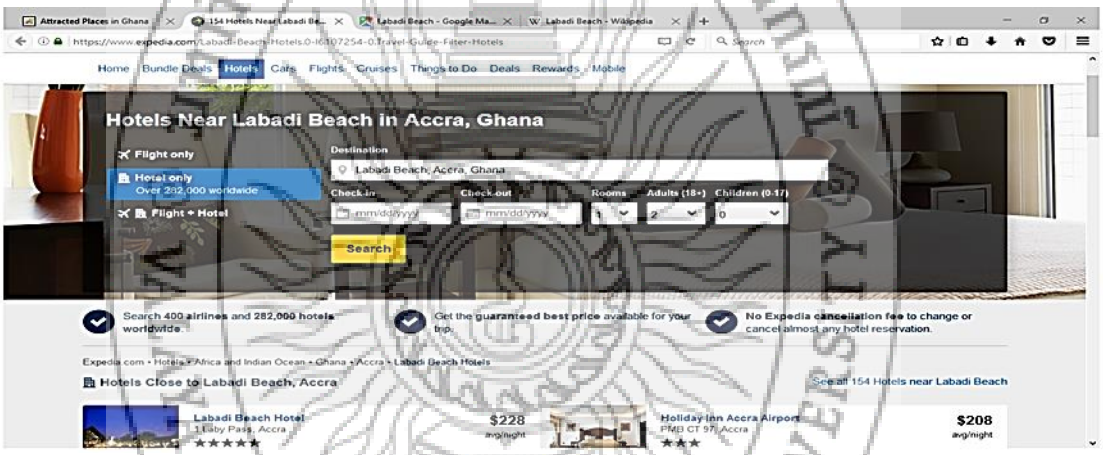

The fig.19 shows the nearby hotels at labadi beach

The example above shows how our system works when user search for an about information Ghana tourism industry. The information Guide system shows the right information the user is looking for since the information guide system has all the nearby information in one platform. From the example above the user ask question about labadi beach and nearby accommodation and our system provided the right information of the User.

C. Evaluation of System by Users

In this study, our system usability is evaluated based on Six Page Tasks and its Task Questions respectively, which are: (1) Ghana Tourism Search engine (2) Fort and Castle (3) About Ghana (4) Hotels (5) Attraction (6) Visa and Diplomatic. The results are assembled and presented in Table III, the percentage of the total tasks mistakes are achieved and represented in the chart given in Fig.10, while the Fig.11 represent the comparison between the overall time and time of mistakes is extracted from the first and third column.

TableII: shows the question and the number that represent it

Task Question(TQ)	**QUERY**
TQ1	Where is labadi beach located?
TQ2	Where is cape coast castle located and it nearest hotels?
TQ3	What is the history of Ghana and attracted places in Ghana.
TQ4	Top 10 hotels in Ghana.
TQ5	Where is the top 10 beaches in Ghana is located and nearby hotels
TQ6	How is the visa issues in Ghana like?

TABLE III RESULTS OF TESTING TABLE

Page Task	Task Question(TQ)	Total Task Time(min)	Total Task Mistakes(num)	Mistake Time (min)
Ghana Tourism Search engine	TQ1	10.3	5	4.2
Fort and Castle	TQ2	5	1	0.5
About Ghana	TQ3	6	1	0.5
Hotels	TQ4	6	1	1
Attraction	TQ5	6	0	0
Visa and Diplomatic	TQ6	5	1	0.5

i) Analysis

The Fig.20 represent the number of mistakes, each of the six page tasks (given in Table III) are displayed by percentages. After we collected the data, we found that First Page task (i.e., Ghana Tourism Search engine) has the most value as compared with other Page tasks. The fifth Page task (i.e., Attraction) has no task mistakes and the other Page tasks (i.e., About Ghana, Hotels, Visa and Diplomatic) has slightly task mistakes.

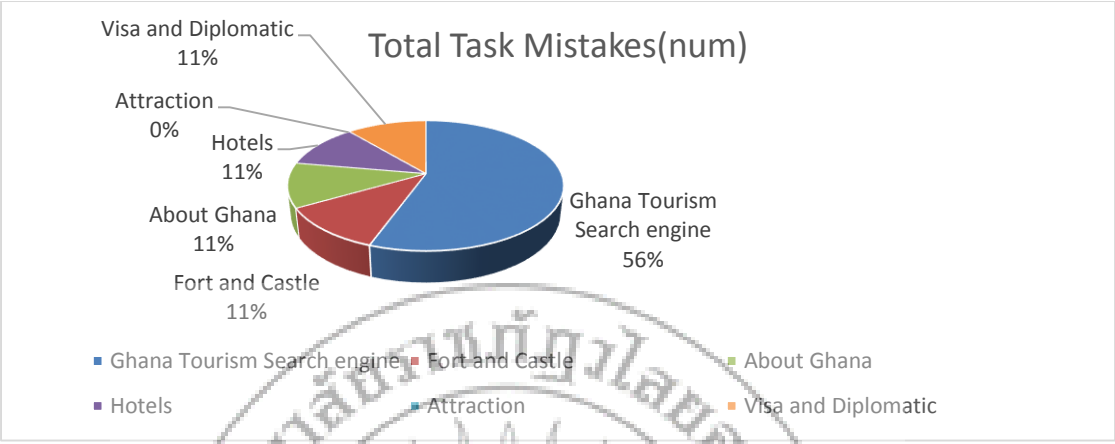

Fig.20 Percentage of Total tasks mistakes

In Page task1 a total of 10.3minutes representing 27.61% of the total task evaluation time. In Page task 2 a total of 5 minutes (13.4%)were spent. 6 minutes (16.09%) were being spent in Page Task 3, 6 minutes (16.09%) were being spent in Page Task 4, 5 minutes (13.4%) were being spent in Page Task 5, 5 minutes (13.4%) were being spent in Page Task 6. The highest ranked Page Task was Page task 1, followed by Page task 4, then Page task 5 whiles page task 6 and page task 2 recorded the same value. The ranking shows how the tasks where easy to the users to performed. The higher ranked show how difficult it was for the users to perform those tasks implying less effectiveness of usage. The total task mistakes made by each tasks were the Page task 1 with 5 mistakes (55.56%) made by users, followed by page task 2, page task 3, page task 4 and also page task 6 with the same mistakes of 1(11.11%) respectively, then page task 5 with no mistakes.

In the evaluation, more mistakes were made by page task 1 showing 5 mistakes (55.56%), followed by page task 2, page task 3, page task 4 and page task 6 with 1 total mistakes (11.11%), lastly page task 2 with no mistake. This shows that Page task 1 causes few difficulties for users to use by users spending much time about 4.2 minutes to fix these errors, followed by page task 2, page task 3, page task 4 and page task 6 with the same mistakes 1(11.11%) respectively but with different time spent in solving them. Lastly page task 5 has no mistakes made by users implying that it was more effectiveness in usage. The time that was used in fixing page task mistakes were less implying that users didn't face too much difficulties doing these page tasks.

With this result, one can conclude that page task 1 cause user's problem to perform and has less effectiveness usage because users sometimes found it difficult to access relevant links provided by Google which causes user a lot of mistakes to refresh the link till they get access by google. This summary indicates that in terms of human computer interaction, user spend less time in getting the need information they are looking for without much difficulties.

Fig. shows the comparison between the overall time and time of mistakes for each of the six page tasks. We found that page task 1 needs enough time to fix a mistakes. The mistakes in other page task doesn't need much time to fix as compared with page task 1. Whiles page task 5(i.e., Attraction) has no mistakes.

Fig.21 Comparison between the overall time and time of mistakes

Summary and Recommendation

In this paper we showed the evaluation of our system using user's evaluation. We used usability testing method to accomplish our task. The method was divided into two phases, a system usability evaluated in accordance to a test plan, while the second phase explains the data received in the test phase. Our system was evaluated based on the six pages of the system. Among all the fact we received from our two charts we concluded that our system stands a great chance of helping users to perform their task easily and less time consuming since one the major aim is to help users searching information about Ghana tourism to get the right information they are looking for and spend less time in searching this information. After we sum up the total of 5 participant time spending on a particular task, we realize our system can help users in spending less time. From the fact we received show that page task1(i.e., Ghana Tourism Search engine) needs enough time to fix mistakes. Based on this, it is recommended that our system should have the paid version of Google Api instead of the free version to allow users to get access to unlimited information and link access since Google did not give all the access to the links that was retrieved from it by user query. For the future work, we plan to add user registration to our system to help us understand user need easily.

References

[1] Mahmudur Rahman (2013) "Search Engines going beyond Keyword Search: A Survey" International Journal of Computer Applications (0975 - 8887) Volume 75 - No. 17
[2] http://aims.fao.org/en/website/AGROVOC- ConceptServer/sub
[3] HarmoNET Ontology Retrieved from:" http://euromuse.harmonet.org/web/guest/23" Last Accessed: 12/10/2015
[4] eTourism Ontology retrieved from:" http://e-tourism.deri.at/" Last Accessed: 12/10/2015
[5] QALL-ME ontology Retrieved from:" http://qallme.fbk.eu/index.php?location=ontology" Last Accessed: 12/10/2015
[6] G.Madhu and Dr.A.Govardhan, Dr.T.V.Rajinikanth" Intelligent Semantic Web Search Engines: A Brief Survey" International journal of Web & Semantic Technology (IJWesT) Vol.2, No.1, January 2011
[7] Wikipedia "Semantic search" Retrieved from:" https://en.wikipedia.org/wiki/Semantic_search" Last Accessed: 9/20/2016.

[8] Sherimon. P.C, Reshmy Krishnan, Vinu.P.V(2012)" Effective Enabling of Sharing and Reuse of Knowledge On Semantic Web by Ontology in Date Fruit Model." IJCSI International Journal of Computer Science Issues, Vol. 9, Issue 3, No 1
[9] Walter Kostiuk" Implementing Commercial Applications with Semantic Search" January 21, 2009
[10] "What is ontology?" Retrieved from: "www-ksl.stanford.edu/kst/what-is-an-ontology.htm" Last Accessed: 27/9/2015
[11] Bhaskar Kapoor and Savite Sharma,(2010) "A comparative study ontology building tools for Semantic Web application" International Journal of web and Semantic Technology(IJWest)Vol.3July.DOI:10.5121/ijwest.2010.1301.
[12] " Custom Search JSON/Atom API" Retrieved from " https://developers.google.com/custom-search/json-api/v1/overview" Last Accessed : 8/9/2016
[13] Harispe S.; Ranwez S. Janaqi S.; Montmain J. (2015). "Semantic Similarity from Natural Language and Ontology Analysis". Synthesis Lectures on Human Language Technologies. 8:1: 1–254.
[14]Ebitisiam K. Elberkawi, Naser .F.M. EL-firjani,Abdelsalam M. Maatuk,Shadi A.Aljawarneh(2016) "Usability Evaluation of Web-based Systems: A New Method and Results" .In proceeding of IEEE ICEMIS 2016

INVESTIGATION OF 4-PORT DIPLEXER FOR BASE STATION

Jessada Konpang, Muhammad Sandhu, Nutapong Somjit and Ian Hunter

Institute of Microwaves and Photonics, School of Electronic and Electrical Engineering,
University of Leeds, Leeds, LS2 9JT, UK

ABSTRACT

Investigation of 4-port diplexer for base station is introduced in this paper. From the analytical solution verified by 3D fullwave simulations, the four-port diplexer can be designed by using two diplexers with 180º different phase. This technique offers the signal isolation of 68.46 dB between transmitter and receiver module, which is the best figure ever reported to date. The four-port network exploits both high and low-Q factor filters for the cost reduction while still offering superior figure-of-merits.

Keywords: Three-port, Four-port, Diplexer, Isolation

Introduction

Generally speaking, the recent advance of radio frequency (RF) and microwave technology has stimulated the rapid development of modern wireless communication systems. For the last few decades, a variety of techniques used to design bandpass filters were developed e.g. lumped-elements (LC Circuit), microstrip configurations, coaxial configurations, dielectric filters, cavity resonator and high temperature superconductors (J.-S. G. Hong and M. J. Lancaster, 2004; I. C. Hunter, L. Billonet, B. Jarry, and P. Guillon, 2002). In microwave system, it is challenging to design a device at low cost and high performance. The design of different filters and diplexers was discussed in (Han-Sam Peng and Yi-Chyun Chiang, 2015; Q. Xue and J.-X. Chen, 2008) which conventional diplexers offer low cost (microstrip structure) but give poor isolation performance (worse than 20dB) and high losses. Consequently, a new technique to improve signal isolation while keeping low signal losses is required. Diplexers are three-port network and commonly used to combine or separate different signal frequencies which they are usually set in the form of filters. RF front-end of a cellular radio base station uses bandpass filters to discriminate two different frequency bands for transmitting (Tx) and receiving (Rx) channels using a single antenna. Generally, relatively high power signals, in an order of 30 W, are generated by Tx channel. Consequently, the Tx filter should have high capability of power handling and the receiver Rx channel has to detect very weak signals (I. Hunter, 2001).

Therefore, in order to protect the low-noise amplifier in the receiver channel from the transmitter channel with high power signals (30 W), the Rx filter is designed to have high signal isolation between the two channels because transmit power amplifier produces out-of-band intermodulation products and harmonics (I. Hunter, 2001). In the transmitting band, Tx filter also has a high level of stopband attenuation to reject the noise generated at the output of the power amplifier. For this reason, diplexer with high isolation between Tx and Rx channels is required.

In this paper, a novel synthesizing technique for interference rejection in future integrated base station is introduced as a superior design technique for the high-isolation at lower cost compared to the state-of-the-art diplexer devices. The proposed

four-port network combines bandpass filters with high and low-Q factor for the cost reduction and device miniaturization while offering superior RF performance.

Analysis of four-port networks

The block diagram of four-port network is shown in Fig. 1.

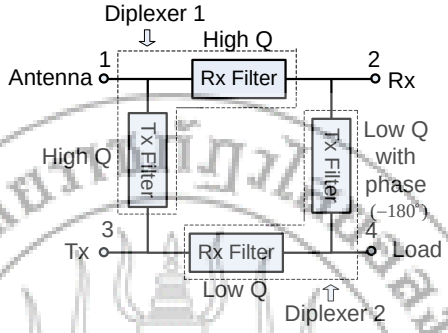

Fig.1. A diagram of four-port network.

From Fig.1, In case of high Q in both paths, we can consider the difference of signal isolation between two paths (3-1-2 and 3-4-2 paths). We can investigate the combination of sine waves as $\sin\theta + \sin(\theta + \Delta)$. Let Δ is phase difference. The comparison between phase and the isolation is shown in Fig. 2. It can be realized that the best signal isolation at Tx and Rx can be obtained from 180° different phase.

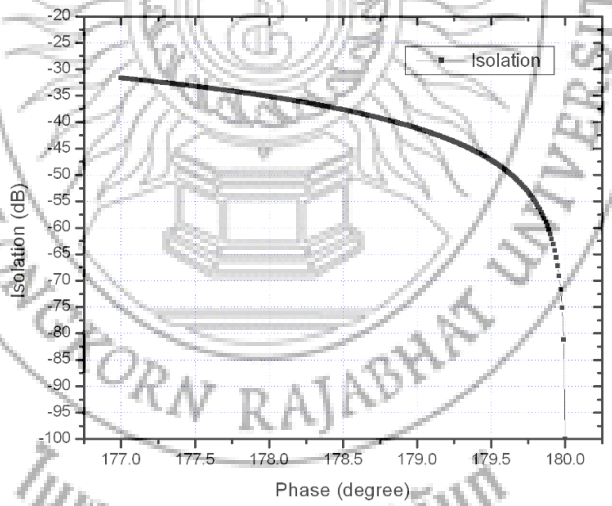

Fig.2. Comparison of isolation response and phase differences.

Lumped-element filter design for diplexer and four-port networks

The key design parameters of lumped-element Chebyshev bandpass filter is shown in table 1.

Table 1. SPECIFCATONS OF BANDPASS FILTERS DESIGN

Centre frequency	Tx=1.73 GHz and Rx=2.13 GHz
Passband Bandwidth	50 MHz
Stopband Attenuation	>40 dB
Passband Return Loss	> 20 dB
Passband Insertion Loss	< 0.4 dB
System Impedance	50 Ω

Firstly, the order of the filter can be calculated in (I. Hunter, 2001).

$$N \geq \frac{L_A+L_R+6}{20\ log_{10}[S+(S^2-1)^{1/2}]} \quad (1)$$

Where

$$L_A=40 \text{ and } L_R=20 \quad (2)$$

S is the selectivity and is the ratio of stopband to passband bandwidth. Hence

$$S=40 \quad (3)$$

$$N\geq =1.734 \quad (4)$$

That is, a degree 2 transfer function at least must be used.

The ripple level ε is

$$\varepsilon = (10^{L_R/10}-1)^{-1/2} \quad (5)$$

=0.1005

Hence

$$\eta = \sinh[\frac{1}{N}sinh^{-1}(1/\varepsilon) \quad (6)$$

=2.1213

And the shunt capacitive element value of the capacitive element Chebyshev low pass prototype is

$$C_r = \frac{2}{\eta}\sin[\frac{(2r-1)\pi}{2N}] \quad (7)$$

Where r=1,…, N

$$C_1 = C_2 = 0.6667$$

The element value of the normalised inverter coupled Chebyshev low pass prototype is

$$K_{r,r+1} = \frac{[\eta^2+sin^2(r\pi/N)]^{1/2}}{\eta} \quad (8)$$

Where r=1,…, N-1

Therefore the inverter value is

$$K_{12} = 1.1055$$

The normalized Chebyshev inverter coupled low pass prototype is represented in Fig. 3.

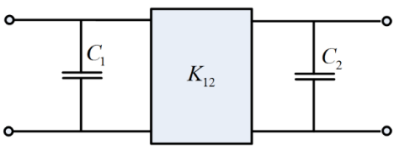

Fig.3. Equivalent circuit of impedance inverter.

At the centre frequency of 1.73 GHz and 2.13 GHz and Z=50 ohm

$$\omega = 2\pi f \quad (9)$$

at 1.73 GHz = 10.87×10^9 and at 2.13 GHz = 13.38×10^9

and $$\alpha = \frac{f}{BW} \quad (10)$$

at 1.73 GHz =34.6 and at 2.13 GHz=42.6

The element values of a lowpass to bandpass frequency and impedance scaled capacitively coupled network shown in Fig. 5 can be calculated as

$$C_{01} = C_{N,N+1} = \frac{1}{\omega Z(\alpha-1)^{1/2}} \quad (11)$$

and

$$C_{r,r+1} = \frac{Kr,r+1}{Z\alpha\omega} \quad (12)$$

Where r=1,…, N-1

The shunt element values can be calculated as

And

$$C_{11} = \frac{\left[\frac{C_1}{\omega} - \frac{(\alpha-1)^{\frac{1}{2}}}{\omega\alpha} - C_{12}\right]}{Z} \quad (13)$$

And

$$C_{NN} = \frac{\left[\frac{C_N}{\omega} - \frac{(\alpha-1)^{\frac{1}{2}}}{\omega\alpha} - C_{N-1,N}\right]}{Z} \quad (14)$$

And

$$C_{rr} = \frac{\left[\frac{C_r}{\omega} - \frac{(\alpha-1)^{\frac{1}{2}}}{\omega\alpha} - C_{r-1,r} - C_{r,r+1}\right]}{Z} \quad (15)$$

Where r=2,…, N-1

$$L_{r,r} = \frac{Z}{C_r\omega} \quad (16)$$

Where r=1,…, N

The element values of second order Chebyshev diplexer are shown in table 2.

Table 2. diplexer design

Elements	Tx=1.73 GHz	Rx=2.13 GHz
$C_{01}= C_{23}$	0.32 pF	0.23 pF
C_{12}	0.06 pF	0.04 pF
$C_{11}= C_{22}$	0.86 pF	0.73 pF
$L_{11}= L_{22}$	6.9 nH	5.6 nH

Design example and results

1.1. Diplexer design

The diplexer (three-port) design is based on the independent design of two bandpass filters as following steps.

Step 1: design filter in Tx at centre frequency of 1.73 GHz with 50 MHz bandwidth.

Step 2: calculate the order of filter and element value of the capacitive element Chebyshev inverter coupled low pass prototype from equation (1) to (8).

Step 3: calculate the element values of a lowpass to bandpass frequency and impedance scaled capacitive coupled network from equation (11) to (16).

The circuit of the capacitively coupled filter network is shown in Fig. 4.

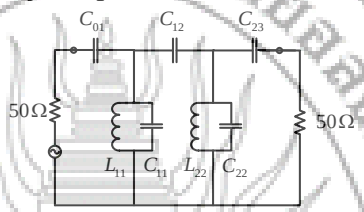

Fig.4. Capacitively coupled filter layout.

Then, the T-junction is connected the two independent bandpass filters together. The circuit of the capacitively coupled diplexer network is shown in Fig. 5. The capacitively coupled three-port network simulated response by AWR microwave office is portrayed in Fig. 6. The 20-dB bandwidth is 50 MHz. The passband IL in Tx band is less than 0.22 dB and Rx band 0.31 dB. The RL in both channels is better than 20 dB in the passband.

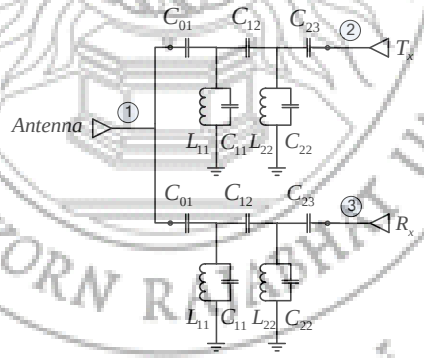

Fig.5. Capacitively coupled diplexer layout.

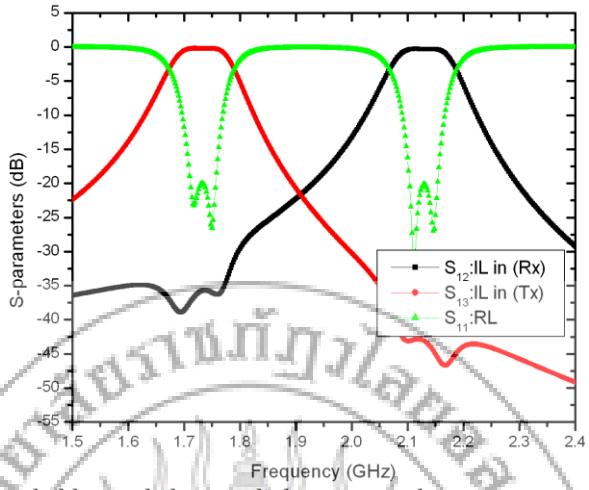

Fig.6. Capacitively coupled lumped element diplexer network response.

1.2. Four-port design

From Fig.1, two diplexer filters (diplexer 1 and 2) are combined together in order to obtain the best isolation. The first diplexer (No. 1, 2 and 3) is designed with High-Q factor (Q=1000). The second diplexer (No. 2, 3 and 4) is designed with Low-Q factor (Q=500). The circuit of the capacitively coupled four-port network is shown in Fig. 7. The capacitively coupled four-port network simulated response is portrayed in Fig. 8. The RL in both channels is better than 20 dB in the passband. The passband IL in Tx band is less than 0.23 dB and Rx band 0.32 dB. It can be seen that both three-port and four port network are almost the same insertion loss. The comparison isolation (S_{32}) of three-port and four-port is shown in Fig. 9. The simulated isolation of diplexer network is 35.66 dB and 68.46 dB in four-port. From Fig. 9, it can be realized that the phase shift between 180º and 183º of four-port network still has signal isolation (S_{32}) better than the existing diplexer (Yonggang Zhou, Hong-wei Deng, and Yongjiu Zhao, 2014; Dong Chen, Lei Zhu, Huizheng Bu, and Chonghu Cheng, 2015).

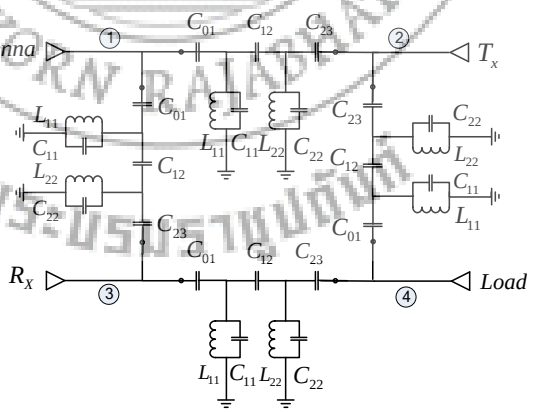

Fig.7. Capacitively coupled four-port layout.

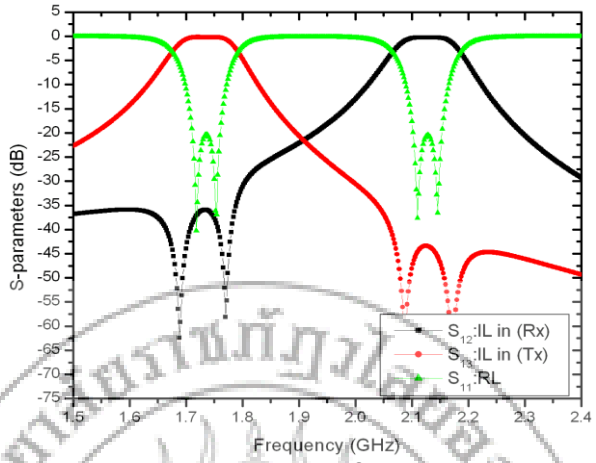

Fig.8. Capacitively coupled lumped element four-port network response.

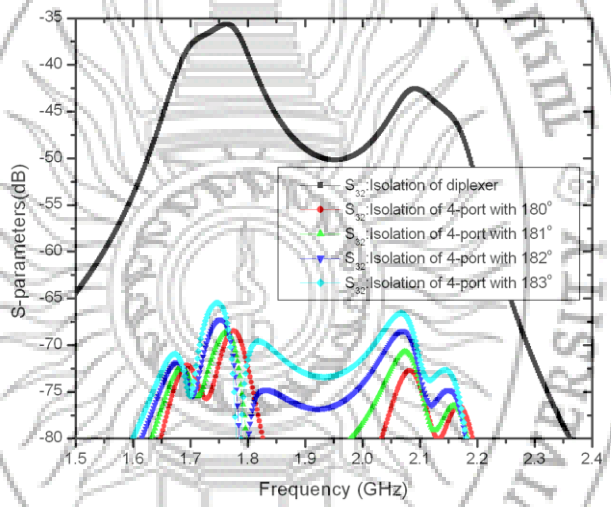

Fig.9. Comparison of isolation (S_{32}) response of diplexer and four-port network.

Summary and Recommendation

The investigation of 4-port diplexer for base station is proposed here. The concept is very attractive since the four-port network is based on the design of two independent diplexer bandpass filters, (Tx at 1.73 GHz, Rx at 2.13 GHz, BW=50MHz): one of them meeting the desired High-Q (Q=1000) and the other desired Low-Q (Q=500). The new technique design can enhance the isolation (S32) from (35.66 dB) to (68.46 dB). Finally, RF interference rejection technique can be used in wireless communication systems whereas small size, low losses and low complexity are required.

References

Dong Chen, Lei Zhu, Huizheng Bu, and Chonghu Cheng. (2015). A Novel Planar Diplexer Using Slotline-Loaded Microstrip Ring Resonator. **IEEE Microwave and Wireless Components Letter**. vol. 25, No. 11, pp. 706-708.

Han-Sam Peng and Yi-Chyun Chiang. (2015). Microstrip Diplexer Constructed With New Types of Dual-Mode Ring Filters. **IEEE Microwave and Wireless Components Letter**. vol. 25, pp. 7-9.

I. C. Hunter, L. Billonet, B. Jarry, and P. Guillon. (2002). Microwave filters-applications and technology. **Microwave Theory and Techniques, IEEE Transactions on**. vol. 50, pp. 794-805.

I. Hunter. (2001). **Theory and design of microwave filters: IET**.

J.-S. G. Hong and M. J. Lancaster. (2004). **Microstrip filters for RF/microwave applications** vol. 167: John Wiley & Sons.

Q. Xue and J.-X. Chen. (2008). Compact diplexer based on double-sided parallel-strip line. **Electronics Letter**, vol. 44, pp. 123-124.

Yonggang Zhou, Hong-wei Deng, and Yongjiu Zhao. (2014). Compact Balanced-to-Balanced Microstrip Diplexer With High Isolation and Common-Mode Suppression. **IEEE Microwave and Wireless Components Letter**. vol. 24, No. 3, pp. 143-145.